Naval Research Laboratory

Washington, DC 20375-5320

Radar Antenna Characterization Using Polarization Measurements

Elaine Chincheck

Airborne EW Systems Branch
Tactical Electronic Warfare Division

August 8, 1994

REPORT DOCUMENTATION PAGE

1. AGENCY USE ONLY (Leave Blank)	2. REPORT DATE	3. REPORT TYPE AND DATES COVERED
	August 8, 1994	August 1992 - August 1993

4. TITLE AND SUBTITLE	5. FUNDING NUMBERS
Radar Antenna Characterization Using Polarization Measurements	PU - ONR/57-3627-A-3

6. AUTHOR(S)

Elaine Chincheck

7. PERFORMING ORGANIZATION NAME(S) AND ADDRESS(ES)	8. PERFORMING ORGANIZATION REPORT NUMBER
Naval Research Laboratory Washington, DC 20375-5320	NRL/FR/5730--94-9588

9. SPONSORING/MONITORING AGENCY NAME(S) AND ADDRESS(ES)	10. SPONSORING/MONITORING AGENCY REPORT NUMBER
Office of Naval Research 800 North Quincy Street Arlington, VA 22217-5660	

11. SUPPLEMENTARY NOTES

12a. DISTRIBUTION/AVAILABILITY STATEMENT	12b. DISTRIBUTION CODE
Approved for public release; distribution unlimited.	

13. ABSTRACT (Maximum 200 words)

The Naval Research Laboratory (NRL) is investigating polarization features of antennas to determine if they can be used for radar identification. This report presents the results of a test under this program whose main objective was to use existing polarization measuring hardware to examine the mainlobe and sidelobe antenna polarization characteristics of different navigation radars and to evaluate how this information can be used for radar identification. A theoretical model was generated to plot the polarization characteristics of slotted waveguide arrays, the type of arrays used in navigation radars. A comparison between theory and real-time measurements was made with encouraging results. This report shows that radars belonging to the same "class" with the same antenna polarization, can be distinguishable when comparing their mainlobe and sidelobe antenna polarization characteristics.

14. SUBJECT TERMS		15. NUMBER OF PAGES
antenna polarization		65
radar identification		**16. PRICE CODE**
navigation radars		

17. SECURITY CLASSIFICATION OF REPORT	18. SECURITY CLASSIFICATION OF THIS PAGE	19. SECURITY CLASSIFICATION OF ABSTRACT	20. LIMITATION OF ABSTRACT
UNCLASSIFIED	UNCLASSIFIED	UNCLASSIFIED	UL

CONTENTS

EXECUTIVE SUMMARY

Modern radars are capable of extracting information from received target echo signals that can be used for target identification and/or electronic counter-countermeasures (ECCM) purposes. One of the concerns of the electronic warfare (EW) community today is on designing EW systems that can identify threat radar systems by using radar characteristics and thus optimize jamming/deception responses. The radar parameter of interest under the effort described in this report is polarization. Radars use polarization to extract target information and/or polarization diversity to minimize jammer effectiveness. In a similar way, EW systems can use radar polarization information to identify radars and optimize jamming and deception waveforms.

The Naval Research Laboratory (NRL) is investigating polarization features of antennas to determine if these features can be used for radar identification. This report presents the results of a test under this program whose main objective was to use existing polarization measuring hardware to examine the polarization characteristics of different navigation radars and evaluate how this information can be used for radar identification.

This program began with the development of a frequency domain polarimeter built by E-Systems, Inc. in 1989. This polarimetric system is unique in that it provides flexibility and simplicity. First, it is flexible because it can be used by EW systems to make accurate assessments, in real time, of the polarization of RF signals. Second, it is simple in that is uses a single-channel receiver, which reduces the cost and weight factors. The frequency coverage of the system is 2 to 18 GHz and it will measure pulsewidths as narrow as 200 ns and pulse repetition intervals as small as 5 μs. The accuracy of the system was determined from laboratory experiments as having a 1 dB amplitude accuracy and a 10° phase accuracy. The 8-bit analog-to-digital converters in the system provide a 0.23 dB amplitude resolution and a 1.4° phase resolution. The sensitivity of the system is -85 dBm and the instantaneous dynamic range is 60 dB. Depending on the frequency of the signal received, the antenna of the polarimeter has a gain ranging from 6 to 23 dBi and a 3-dB beamwidth from 67° to 6°.

To measure polarization, the ratio of the amplitudes of any two orthogonal linear polarization components of the electromagnetic field and their relative phase must be known. The orientation chosen for this polarimeter is to measure the 45° and 135° slant linear components of the wave. It accomplishes this by measuring polarization of an incident electromagnetic wave from the frequency spectrum of the received and specially processed signal. This is done by rapidly switching between the two ports of a dual-linearly polarized quad-ridged horn antenna, which, in the frequency domain, creates a carrier signal containing the 45° slant component information (amplitude B), and sideband signals containing the 135° slant component information (amplitude A). The polarization information is extracted from the frequency spectrum representation of the switched signal. Each pulse is measured once. The phase measurement made by the polarimeter is called the time-phase. This is the phase relationship between the 45° (carrier) and 135° (sideband) slant components in the time dimension (i.e., the dimension in which the wave is travelling).

E-1

For the main polarizations, the polarimeter provides the following values for the two amplitude (A and B) and one phase (ϕ) measurements:

45° slant	$A < B$	ϕ = undefined
135° slant	$A > B$	ϕ = undefined
Vertical	$A = B$	$\phi = 0°$
Horizontal	$A = B$	$\phi = 180°$
Right-hand circular	$A = B$	$\phi = 90°$
Left-hand circular	$A = B$	$\phi = 270°$

In theory, polarization of an electromagnetic wave is emitted from a slotted waveguide similarly to the way it is emitted from a dipole; because there is no cross-polarization component of the wave in the principal plane, the wave is completely copolarized. However, as the angle off boresight increases, a cross-polarization component exists which changes the cross-polarized-to-copolarized ratio and, hence, changes the polarization of the wave. For example, for an emitter horizontally polarized on boresight, when the cross-polarization component (vertical) off boresight equals the copolarization component (horizontal), the polarization of the wave would be 45° slanted. There is a difference in the polarization from the backlobes between a dipole and a slotted waveguide. The polarization emitted from a dipole has the same pattern on both sides of the dipole. For the slotted waveguide, however, the polarization emitted from the side of the waveguide containing the slots is different from that emitted from the back of the waveguide, which contains no slots.

A field test was conducted to evaluate the antenna polarization characteristics of various navigation radars. The test was performed in August 1992 at the Naval Air Warfare Center - Aircraft Division (NAWC-AD), Patuxent River, MD. The intent of this test was to measure and analyze antenna polarization characteristics to evaluate (a) scan-to-scan characteristics from the same radar unit, (b) position-to-position characteristics from the same radar unit, and (c) radar-to-radar comparison. The approach used was to measure the antenna polarization of two navigation radars (FR602D) with the same antenna model and one navigation radar (FR8100) whose antenna is different from the other two. The measurements were done with the navigation radars on boats positioned in each of three designated locations in the Chesapeake Bay and with the polarimeter on a stationary land site. The two FR602D radars were on different boats. The boats were pointing south while at all locations, although the exact angle heading was not measured. Each radar was measured independently (i.e., one radar was turned on at a single time) and the antennas were rotating at a constant rate of 24 rpm. For each data collection, the antenna of the polarimeter was aimed at the vessel which carried the radar antenna being measured.

There are several differences between these two radar models that are important to polarization measurements. The FR602D radar is enclosed in a radome, which depolarizes to some degree the field emitted, whereas the FR8100 radar is an open radome antenna. The FR602D has a smaller radiator (80 cm) than the FR8100 (200 cm), which causes a difference in copolarization-to-cross-polarization ratio in the sidelobes. The beamwidth of the FR8100 antenna is smaller in both the horizontal and the vertical directions, giving this radar a longer detection range (72 nmi).

The polarimeter collects pulses for 50 ms and processes them for another 50 ms. During the 50 ms processing time when the polarimeter is not collecting data, the radar being measured continues to rotate. This may sometimes cause the polarimeter to miss data from the mainbeam of

the antenna when the rotation rate is fast (2.5 s per revolution), as was the case in this test. The measured radars rotated 7.2° during the 50 ms processing time and the polarimeter missed the mainbeam in some of the data collected.

The frequencies of the radars measured are within 10 MHz of each other, as are most navigation radars. Therefore, in the data collected there were times when pulses from more than one emitter were collected. To properly represent the polarization characteristics of the radars measured, a sorting routine was implemented to filter out the interference data.

Figure E1 illustrates some of the measurements made from this test. Data are presented in groups of three: a power measurement, an amplitude difference measurement, and a phase difference measurement. In Fig. E1, (a) through (c) show one revolution from each radar at location 2 and (d) through (f) show one revolution from each radar at location 3. In each figure, the top plot shows the power of the signal, the middle plot shows the difference-in-magnitude, and the bottom plot shows the time-phase.

The first phase of the test evaluated the characteristics of multiple scans of the same radar to evaluate the consistency in antenna polarization characteristics from scan to scan. The results from the scan-to-scan test showed that the scans of a radar possess the same polarization characteristics with only slight variations. For both radars, the measured data indicated good polarization measurements for areas of the revolution where the power of the received signal was high (mainbeam). The measurements showed that in areas of the revolution where the power was low (sidelobes), the polarization was variable. This was evident by the large difference in the magnitude of the two orthogonal components, an indication that the polarization measured was more slant-polarized (i.e., +45° or 135°) than horizontal. These characteristics agree with the theory on dipole polarization, where the ratio of the copolarization component to the cross-polarization component of the electromagnetic wave transmitted from a dipole decreases as the angle off boresight increases. Hence, the polarization varies in the sidelobes for this type of antenna. Two FR602D radars were measured in this test. From this test alone, it is impossible to discern which of the two FR602D radars tested originated the signal. Better controlled tests may reveal differences in polarization of the scans of two of the same type radars.

The second phase of this test compared the antenna characteristics of the same radar from three different geographical positions to see whether multipath affected the measured polarization. As can be seen in Fig. E1, the polarization characteristics of this radar follow approximately the same pattern in positions 2 and 3, and, hence, it can be identified as potentially the same radar despite the location.

There were some slight variations between the locations, for which there are several possible explanations. One is that the orientation of the vessel relative to the polarimeter caused the field from the antenna to bounce off different objects on the vessel. The height of the antenna above sea level may also contribute to these differences; the FR8100 radar was higher than the FR602D radars and the boat which carried the FR8100 radar, the *Transporter*, is larger than the boats which carried the FR602D radars (i.e., the *Prince* and the *Septar 06*). A fourth possibility is that a passing vessel may cause a wake in the water's surface that would change the multipath environment and affect the polarization of the electromagnetic wave. All of these uncertainties could be answered with further testing under stricter testing conditions.

The third phase of the test compared the antenna polarization characteristics of two different radar models. A visual comparison of the antenna polarization characteristics of the FR8100 radar to those of either of the two FR602D radars reveals that the polarization characteristics are significantly different. The main factor contributing to these differences is the number of slots in the waveguide of the antenna; there are approximately 25 slots in the FR602D radar and approximately 100 slots in the FR8100 radar. The radiation from each slot in edge-slot waveguides has the same characteristics as dipoles. As the number of dipoles and, hence, the number of slots in the array increases, the ratio of copolarization to cross-polarization changes (the copolarization component decreases more rapidly with a larger number of elements). Other differences in the design of the radars that may be contributing factors to the polarization characteristics of the antenna are dome features, horizontal beamwidth, and location of the electronics for each radar.

This test contributed a significant insight to using antenna polarization as a means of radar recognition. It is possible from these test results to tell which revolution of data came from the FR602D radar and which came from the FR8100 radar. It is not possible, however, with current data processing, to determine from which of the two FR602D radars a measured signal came. Making this distinction will require further data processing, the next phase under this program.
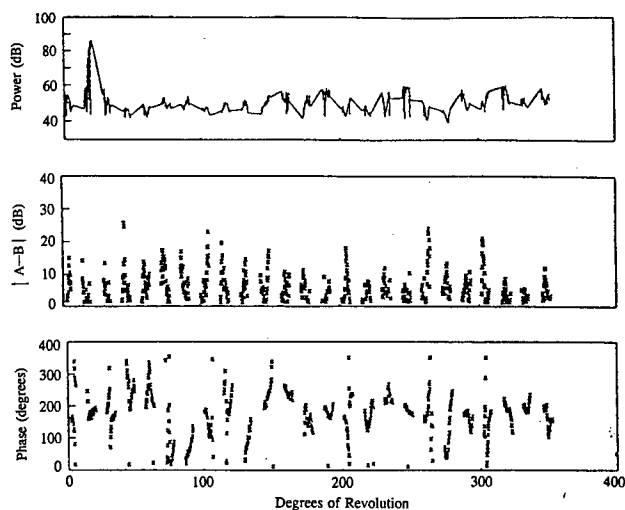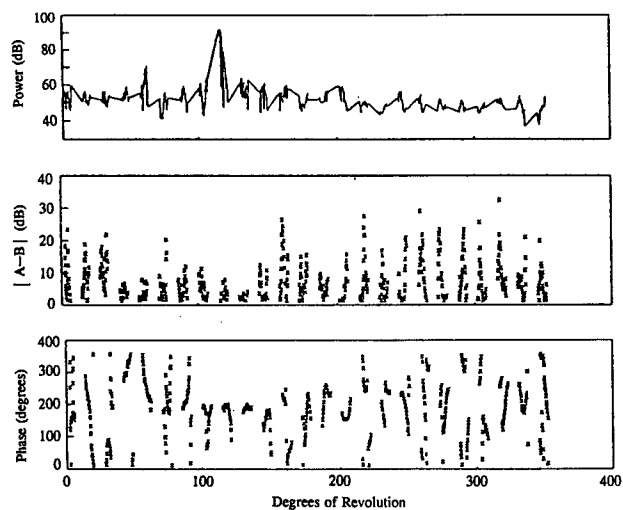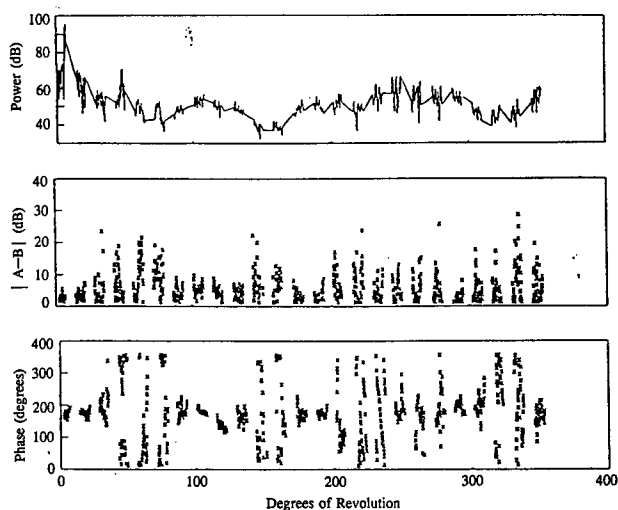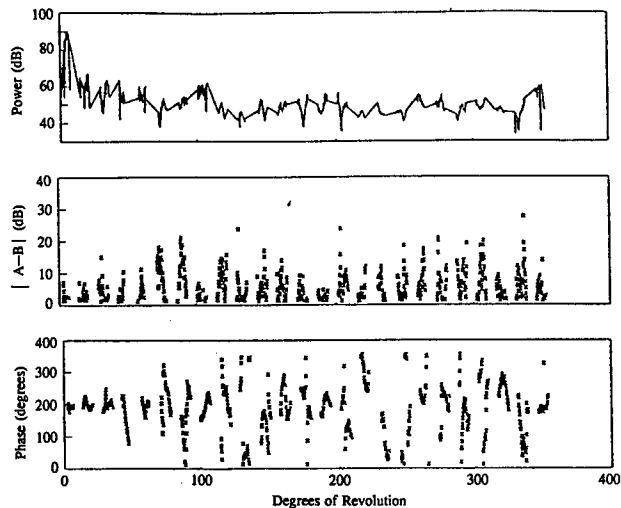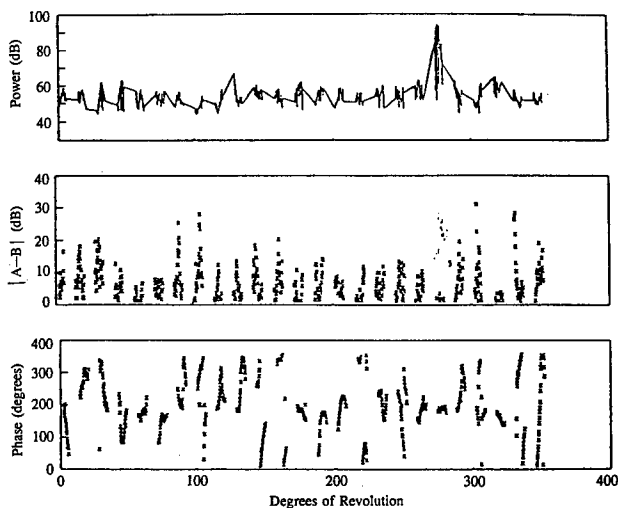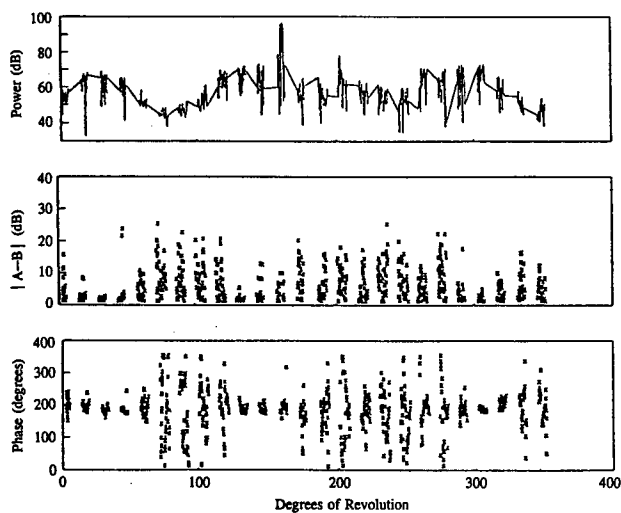
(a) FR602D radar on *Septar 06* in position 2

(b) FR602D radar on *Prince* in position 2

(c) FR8100 radar on *Transporter* in position 2

(d) FR602D radar on *Septar 06* in position 3

(e) FR602D radar on *Prince* in position 3

(f) FR8100 radar on *Transporter* in position 3

Fig. E1—Summary of measured data

E-5

RADAR ANTENNA CHARACTERIZATION USING
POLARIZATION MEASUREMENTS

1. INTRODUCTION

Modern radars are capable of extracting target information from received target echo signals for use in target identification (noncooperative target recognition, NCTR) and electronic counter-countermeasures (ECCM) [1,2,3]. The parameters that can be extracted from a target by radars include location in range and angle, shape and how it changes, size, type of engines, roughness or edginess (polarization backscattered energy), nonlinearity of metal contacts, and speed, course, and maneuver [4]. The electronic warfare (EW) community today is less concerned with how well the NCTR radars work than with how these radars impact existing and future EW systems. The question is how can the EW systems exploit radar characteristics to perform their own NCTR on threat radar systems so that they can optimize their jamming and deception responses.

The radar parameter of interest under the effort described in this report is polarization. Radars use polarization to extract target information and/or polarization diversity to minimize jammer effectiveness. Similarly, EW systems can use radar polarization information to identify radars and to tailor their jamming and deception waveforms to counter these specific radars. The effort described herein addresses this problem.

A program is in place at the Naval Research Laboratory (NRL) to investigate polarization features of antennas and analyze measured data to determine if radar identification is feasible. This report presents the results of a test run under this program whose main objective was to use existing polarization measuring hardware to examine the polarization characteristics of different navigation radars and to evaluate how this information could be used for radar identification purposes.

Section 2 briefly describes general polarization theory. Section 3 explains the theory behind the technique used to collect the information. Section 4 describes the polarimeter operation and its tuning procedures, specifications, and the form of the output data. Section 5 describes the experimental arrangement and summarizes the tentative results. Section 6 draws tentative conclusions from the test and Section 7 recommends further investigations in the area of radar identification with polarization information.

2. POLARIZATION THEORY

The polarization of an electromagnetic field is defined as the direction of its electric field vector E. The direction chosen in this report to illustrate polarization will be vertical. Figure 1 is a snapshot of a vertically polarized wave at one instant of time as it propagates in the direction normal to the phase front [5]. The phase front plane can be considered as a stationary plane of

observation through which the wave moves. As time goes on, the propagating wave moves through the observation plane and the amplitude of the observed E-field vectors varies sinusoidally with time. Figure 2 presents a more simplistic way of illustrating the plane wave for a vertically and a horizontally polarized wave.
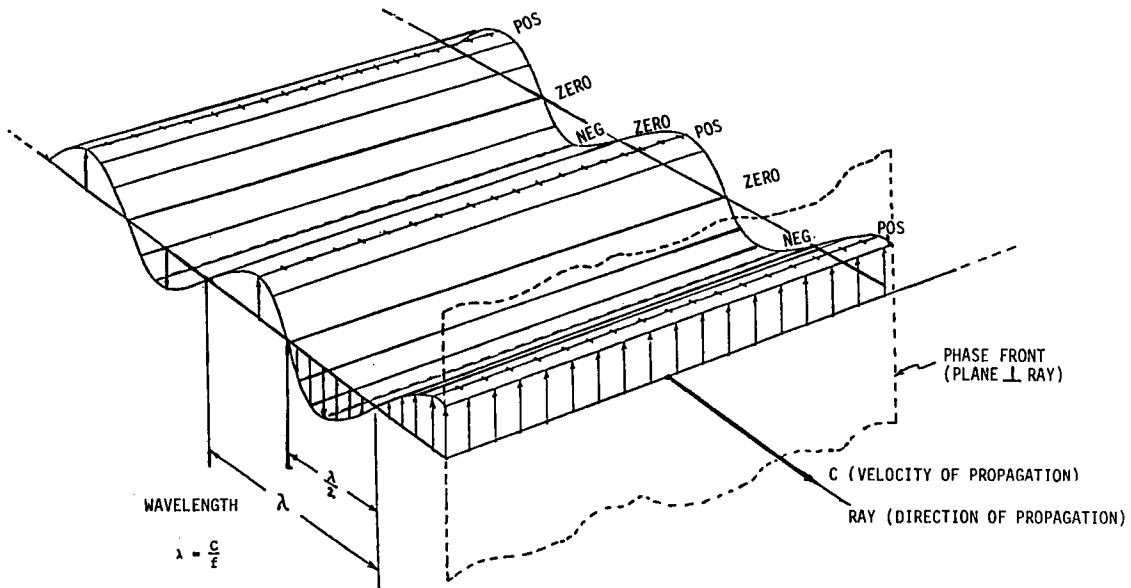

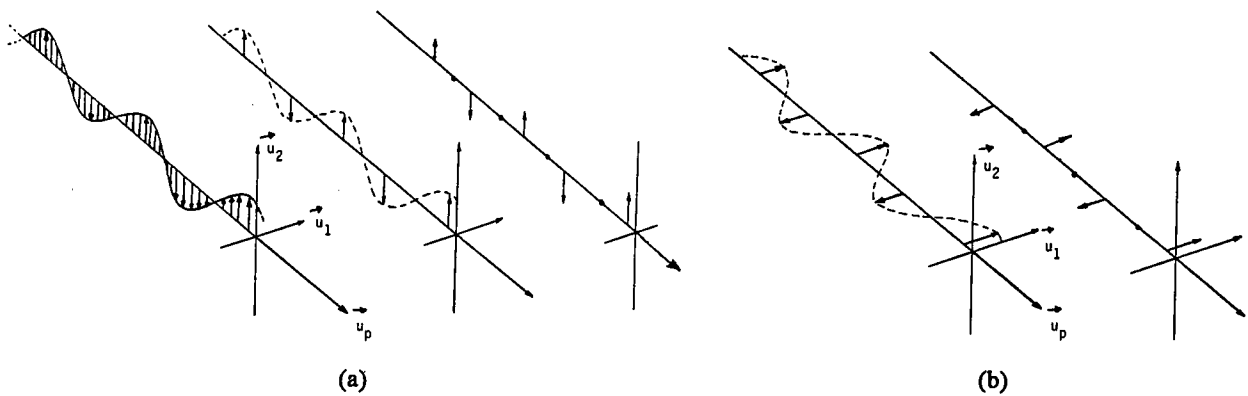Fig. 1—Electric field distribution of a plane wave in space at one instant of time

Fig. 2—Abbreviated diagram of (a) vertically and (b) horizontally polarized plane waves (E-field only)

Any vector of the electric field passing through the observation plane can be synthesized by superimposing two orthogonal linear vectors. When these orthogonal vectors represent waves (as in Fig. 2) that are phase coincident (0° phase difference between them) as they travel through time, the result is a linear polarization vector which is the sum of the two orthogonal linear vectors, shown in Fig. 3. If the waves are not in-phase, however, and the magnitudes of the two orthogonal vectors are not equal, the result is an elliptically polarized wave, because the vectors passing through the observation plane trace an ellipse, as shown in Fig. 4. For the instant shown in Fig. 4, at time $\omega t = 0$, only a horizontal vector exists (Fig 4(b)) representing vectors 1, 5, or 9. One-quarter cycle later ($\omega t = 90°$), the negative peak vertical component has reached the observation plane and hence the result is as shown in Fig. 4(c). This vector represents vectors 2 or 6. As the vectors shown pass through the observation plane, an ellipse is traced, hence the term elliptical polarization. It should be noted also that looking towards the approaching wave, the wave appears to rotate clockwise, which according to the IEEE definition is considered left-hand elliptical polarization. Counter-clockwise rotation, similarly, is called right-hand elliptical polarization. If the vectors are of equal amplitude, then they will trace a circle instead of an ellipse; this is called circular polarization.
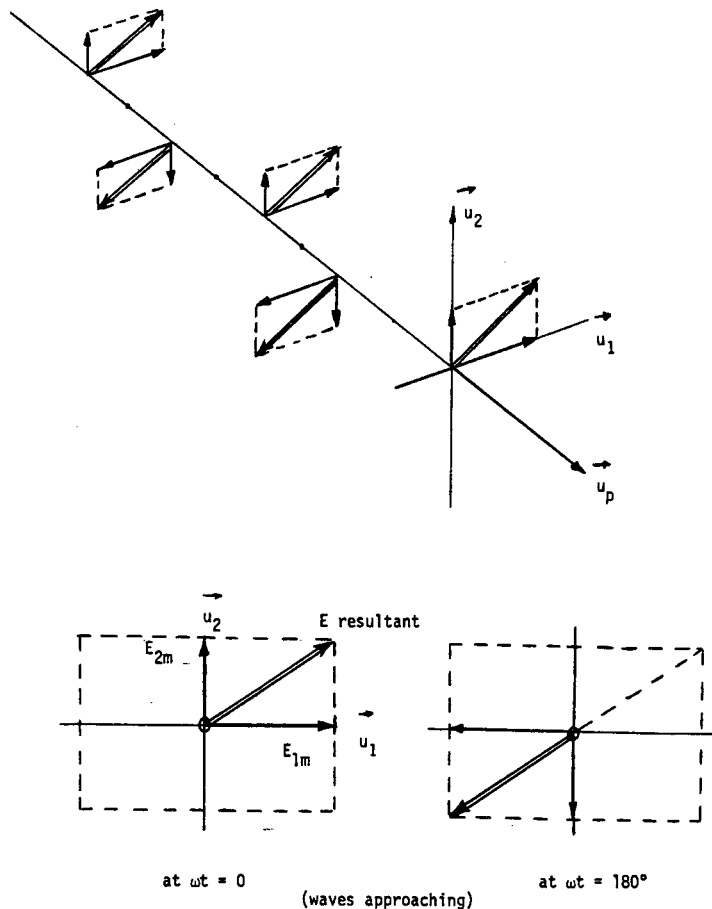

Fig. 3—Superposition of vertical and horizontal plane waves in phase coincidence, producing tilted linear result
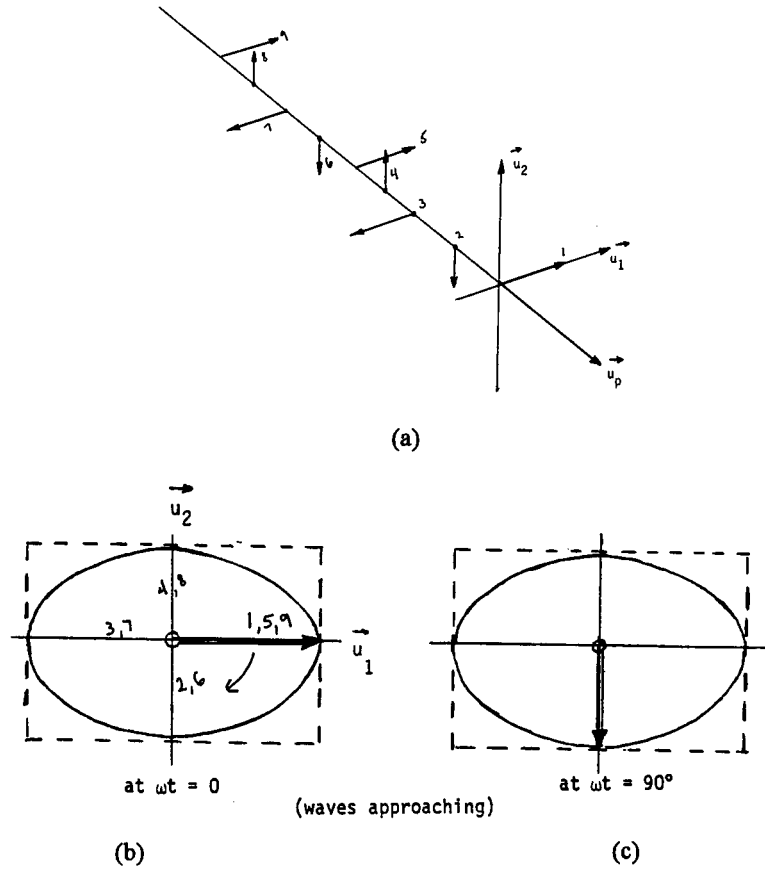
(a)

(waves approaching)

(b)   (c)

Fig. 4— Superposition of orthogonal linear plane waves with
phase quadrature, producing elliptical result

Several methods are available for measuring polarization [2]. One of them is to measure the ratio of the amplitudes of two orthogonal linear polarization components of the field and their relative phase. These components may be of any orthogonal orientation. The orientation chosen for this polarimeter design is to measure the 45° and 135° slant linear components of the wave. For a perfect 45° slant-polarized wave, only a 45° vector component exists and, hence, one output from the polarimeter, the 135° representative vector, will be zero. For a 135° slant-polarized wave, the 45° vector component will be zero. In the cases of vertical, horizontal, right- and left-hand circular polarizations, the 45° and 135° slant components are equal in magnitude, as discussed further in the following section.

3. THEORY OF POLARIMETER OPERATION

The theory behind this experiment is focused on the methodology used to measure polarization variations and properties of signals received from the antenna sidelobes and backlobes. Although Section 5 explains the theoretical response from the two antenna structures measured, this report does not focus on explaining and/or providing a physical reasoning on the polarization behavior of different antenna structures, but rather on the phenomenology of measuring different polarizations, no matter how they are generated.

This program began with the development of a "frequency domain polarimeter" built by E-Systems, Inc. in 1989. This polarimetric system is unique in that it provides flexibility and simplicity. First, it is flexible because it can be used by EW systems to make accurate assessments, in real time, of the polarization of RF signals. It does this by measuring polarization of an incident electromagnetic wave from the frequency spectrum of the received and specially processed signal. This is done by rapidly switching between the two ports of a dual-polarized antenna, which, in the frequency domain, creates a carrier signal and sideband signals on the single channel of the polarimeter. The polarization information is extracted from the frequency spectrum representation of the switched signal. This information can be used for effective threat identification, jamming, and deception purposes. Second, it is simple in that it uses a single-channel receiver. This feature reduces the cost and weight factors that have been of major concern and a deterrence to using polarization detection in electronic warfare systems.

Before explaining the detailed operation of the frequency-domain polarimeter, a representation of different signals in the frequency domain is provided. The purpose of this is to refresh the reader's memory on frequency spectrum signal representation, the basis for the operation of the polarimeter. Table 1 shows some basic time-domain functions and their equivalent frequency-domain representations (i.e., Fourier transforms) [6]. Also, the Appendix of this report should be reviewed prior to reading the theory of operation. This Appendix shows the mathematical derivation of the frequency spectrum interpretation.
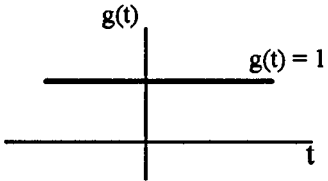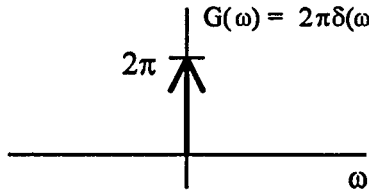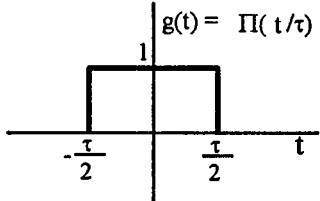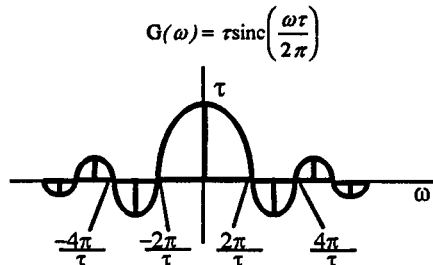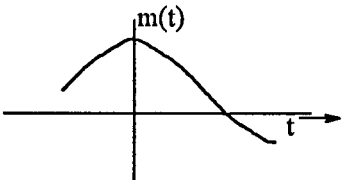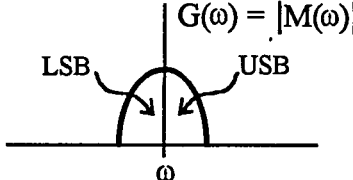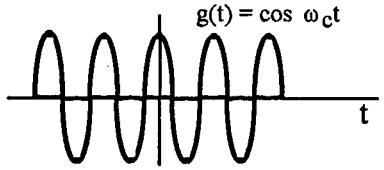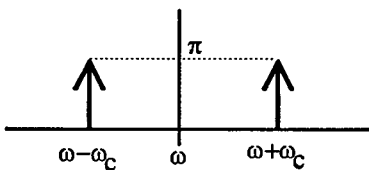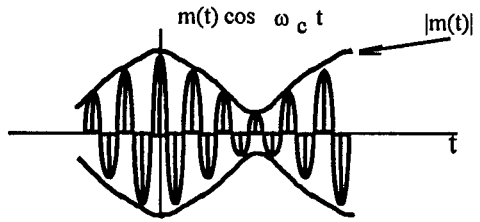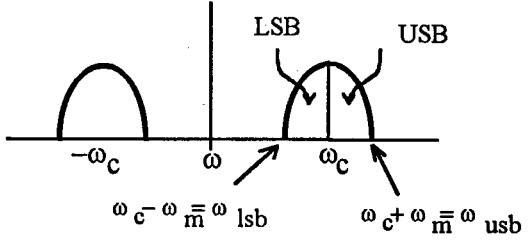
The frequencies presented in Table 1 are ω_c, ω_m, ω_{usb}, and ω_{lsb}. ω_c is the frequency of the carrier signal, $\cos \omega_c t$; ω_m is the frequency of the modulating signal (i.e., the frequency at which the switch at the output of the polarimeter antenna operates); ω_{usb} and ω_{lsb} are the upper sideband and lower sideband frequencies. The data processing portion of the polarimeter stores the 45° slant information at ω_c and the 135° slant information at ω_{usb}. The information at ω_{lsb} is the same as that at ω_{usb} and, therefore, only ω_{usb} information is used for the processing. Hence, $\omega_s = \omega_{usb}$.

3.1 Amplitude Measurement

45° Slant Polarized Wave

Figure 5 presents a scenario in which an incident plane wave, with a 45° slant polarized electric field vector, E_{45}, is received by two linear orthogonal antennas mounted in vertical and horizontal positions, A_V and A_H, as in the polarimeter antenna.

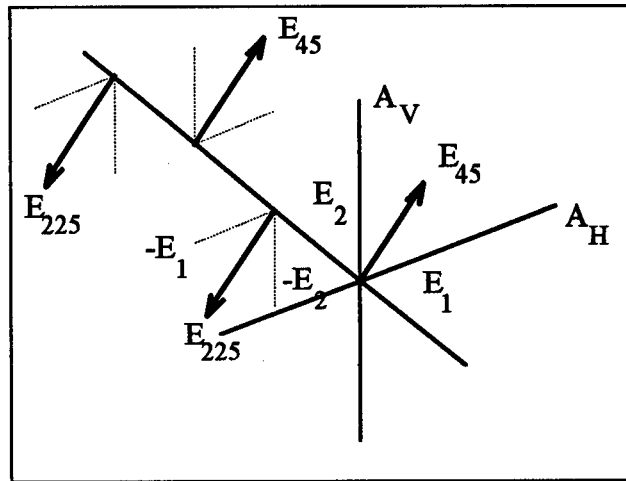**Table 1—Some Examples of Time-Domain Functions and Their Fourier Transform Representation**

Time-Domain Function	Frequency-Domain Function
Function 1 : Constant (dc) $g(t)$ $g(t) = 1$ t	$G(\omega) = 2\pi\delta(\omega)$ 2π ω
Function 2 : Gate Function $g(t) = \Pi(t/\tau)$ 1 $-\frac{\tau}{2}$ $\frac{\tau}{2}$ t	$G(\omega) = \tau\,\mathrm{sinc}\left(\dfrac{\omega\tau}{2\pi}\right)$ τ ω $\dfrac{-4\pi}{\tau}$ $\dfrac{-2\pi}{\tau}$ $\dfrac{2\pi}{\tau}$ $\dfrac{4\pi}{\tau}$
Function 3 : modulating signal $m(t)$ t	$G(\omega) = |M(\omega)|$ LSB, USB ω
Function 4 : carrier signal only $g(t) = \cos\omega_c t$ t	$G(\omega) = \pi[\delta(\omega-\omega_c) + \delta(\omega+\omega_c)]$ π $\omega-\omega_c$ ω $\omega+\omega_c$
Function 5 : carrier signal modulated by m(t) $m(t)\cos\omega_c t$ $|m(t)|$ t	$G(\omega) = 0.5[M(\omega + \omega_c) + M(\omega - \omega_c)]$ LSB USB $-\omega_c$ ω ω_c $\omega_c - \omega_m = \omega_{lsb}$ $\omega_c + \omega_m = \omega_{usb}$

$$|E_1| = .707 \ |E_{45}|$$
$$|E_2| = .707 \ |E_{45}|$$

Fig. 5—45° Polarized electric field vector incident on dual-polarized antenna

Sending both outputs of the antenna (E_1 and E_2) into an ideal sampler, which switches instantaneously from one antenna element to the other, results in a continuous wave of constant amplitude. Regardless of which portion of the 45° slant polarized wave crosses the observation plane, the vector components of the observed vector are always in phase with reference to antenna ports 1 and 2. Figure 6 shows the polarimeter sampled time signal for a 45° slant polarized wave.
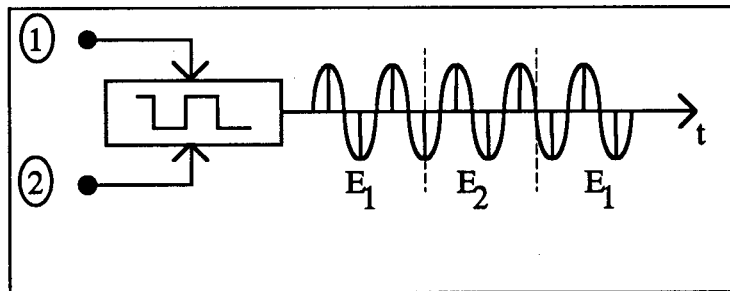

Fig. 6—Sampled time signal of 45° polarized vector received on dual-polarized antenna

The signal in Fig. 6 is similar to what the received signal would look like if the polarimeter antenna had a single, and similar, polarization as the received signal. In Fig. 6, the magnitudes of E_1 and E_2 are equal and are 3 dB lower than the magnitude of E_{45}. Only one frequency, the carrier frequency which is also the radio frequency of the emitter, is present in the signal in Fig. 6. This is represented by a single spectral line in the frequency domain shown in Fig. 7. The magnitude of this spectral component is designated as the B output of the polarimeter. The other output, magnitude A, which represents the harmonics (i.e., the sideband information) is described later. The Appendix provides a detailed mathematical derivation of the spectral representation.
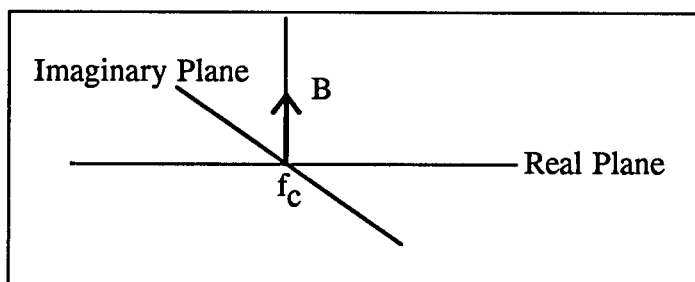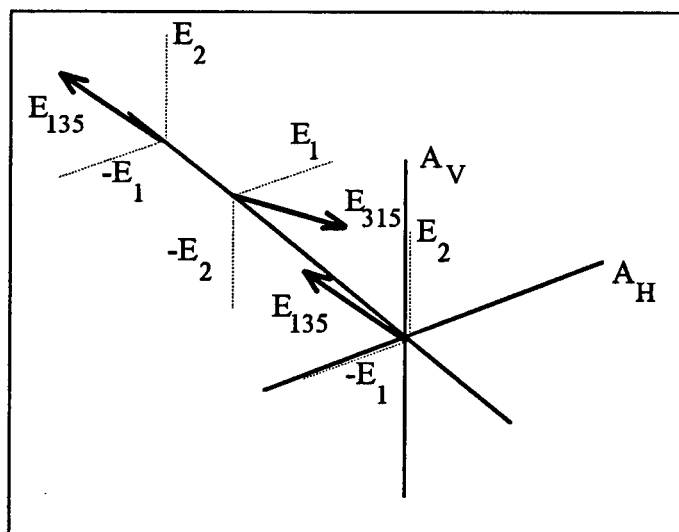
Fig. 7—Spectral representation of a 45° polarized vector received on a sampled dual-polarized antenna

The presence of a carrier frequency (output B) with no secondary frequencies or harmonics, as in the case pictured in Fig. 7, tells us that the polarization of the signal received is equally measured in magnitude and phase on the two antenna ports of the polarimeter. For a dual-polarized antenna whose ports are vertical and horizontal, this is possible only for a 45° slant polarized wave. Therefore, the spectrum of the carrier signal depicted in Fig. 7 represents the 45° component of the incident wave, which in fact is the only component of the received signal.

135° Slant Polarized Wave

If the incident plane wave has 135° slant polarization, then the antenna outputs are as shown in Fig. 8, and the switched, time-sampled outputs are as shown in Fig. 9. Note that, in this case, no matter which portion of the wave passes the observation plane, one of the vector components of the vector at the observation plane is 180° out-of-phase with one of the antenna ports (i.e., for E_{135}, $-E_1$ is 180° out-of-phase with $+E_1$ and for E_{315}, $-E_2$ is 180° out-of-phase with $+E_2$).

$$|-E_1| = .707 \, |E_{135}|$$
$$|E_2| = .707 \, |E_{135}|$$

Fig. 8—135° Polarized electric field vector incident on dual-polarized antenna
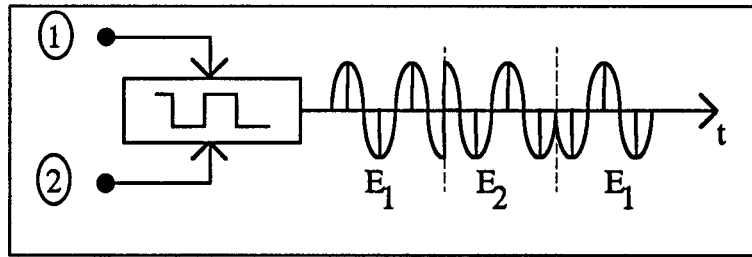
Fig. 9—Sampled time signal of 135° polarized vector received on dual-polarized antenna

It is shown in the Appendix that in the frequency domain, this time-sampled 135° slant polarized signal yields no signal at the carrier frequency, but does yield sideband signals, which are designated as the *A* output of the polarimeter, as shown in Fig. 10.
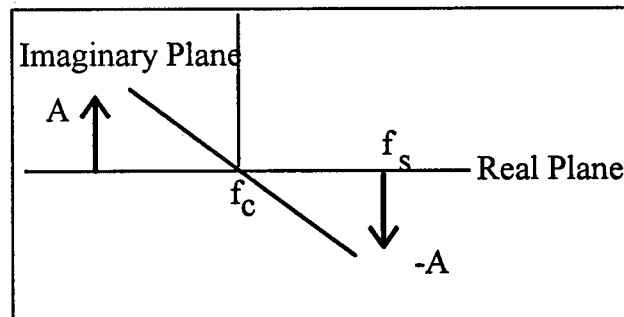
Fig. 10—Spectral representation of a 135° polarized vector received on a sampled dual-polarized antenna

The fact that a 45° slant wave generates a carrier signal and no sidebands, and that a 135° slant wave generates sidebands and no carrier is key to the operation of the single-channel polarimeter. By looking in the frequency domain, at carrier and sideband components (amplitude as well as phase difference), one is effectively resolving any signal into 45° slant and 135° slant polarization components. The frequency-domain characterization of signals with other polarization characteristics is discussed further below.

Vertically Polarized Wave

Looking at a case where a vertically polarized electric field vector E_V is received by the same dual-polarized antenna as described above, the incident plane wave is received as shown below in Fig. 11.
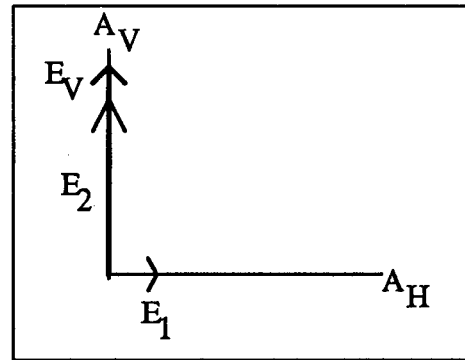
Fig. 11—Vertically polarized electric field vector incident on a dual-polarized antenna

In an ideal condition, $E_1 = 0$. For the purpose of explaining the theory, a nonideal condition will be assumed where a small amount of E_1 is received on the horizontal port of the antenna. Sending both outputs of the antenna, E_1 and E_2, into an ideal sampler results in the signal shown below in Fig. 12.
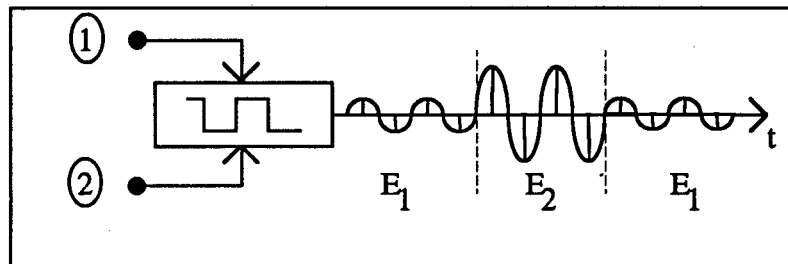
Fig. 12—Sampled time signal of vertically polarized vector received on a dual-polarized antenna

In this case, the magnitudes of E_1 and E_2 are not equal. The phase of the signal in Fig. 12 is still continuous, making E_1 in phase with E_2. The signal depicted above looks like an amplitude modulated (AM) wave or more specifically, an ON/OFF keyed (OOK) signal. As shown in Table 1, a signal combined with a modulated waveform has two frequencies: one is the RF of the emitter (f_c) and the other is the frequency of the OOK signal. Figure 13 is the spectral representation of the signal in Fig. 12.
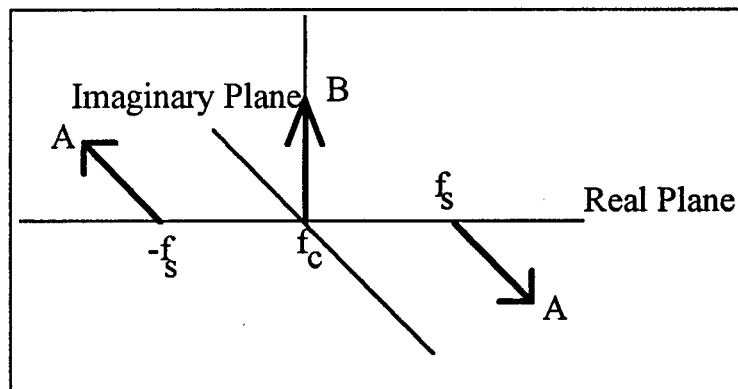
Fig. 13—Spectral representation of a vertically polarized vector received on a dual-polarized antenna

The carrier frequency spectral component provides information about the 45° slant component of the wave received at the polarimeter, as in the previous case. The signals offset by the modulation frequency, i.e., the sidebands, provide information about the 135° slant component of the incident wave, which is equal in magnitude to the 45° component for a 100% vertically polarized wave.

Using this same technique for some of the other common polarizations, Table 2 shows what the output of the polarimeter would be for horizontal, vertical, 45° slant, 135° slant, right-hand circular, and left-hand circular polarizations.

3.2 Time-Phase Measurement

The phase measurement made by the polarimeter is called the "time-phase." This is the phase relationship between the 45° (B or carrier) and 135° (A or sideband) slant components in the time dimension (the dimension in which the wave is travelling). Note that the phase difference between the A and B outputs is quite different from the phase difference between signals from the two antenna ports. To make a time-phase measurement, two signals must be present. In the case of a 45° slant wave, since only one frequency (f_c) is present, no phase measurement can be made between B (the carrier) and A (the sidebands). If a small amount of A is present, since the polarization of an emitted field is never perfect, then a phase difference will exist between the two components and, hence, a phase measurement will be possible. Since the presence of a sideband varies based on the unstable polarization of the emitted field, the phase measurement between B and A varies for a 45° slant polarized wave and is, therefore, undefined. To summarize, the output of the polarimeter measuring a 45° slant polarized wave has a large B component, a small A component (i.e., harmonics) or none at all, and a variable phase difference. The same considerations apply for a 135° slant polarized wave with harmonics but little or no carrier.

The 45° and 135° slant components for a vertically polarized wave are always in-phase with the antenna ports, so the time-phase measurement for a vertically polarized wave is 0°. For a horizontally polarized wave however, one of the components of the field passing the observation plane at any time will always be 180° out-of-phase with respect to one of the antenna ports, yielding 180° time-phase measurement for horizontal polarization. For right-hand and left-hand circular polarizations, the 45° and 135° components are either 90° or 270° out-of-phase with respect to the antenna ports. The phase is measured in the IF section of the polarimeter, where the carrier is coherently beat down to the sideband frequency, allowing the relative phase between the 45° and 135° frequency components to be measured.

4. DESCRIPTION OF POLARIZATION MEASUREMENT SYSTEM

This section summarizes the operation of the Frequency Domain Polarimeter by first discussing the operation of the hardware, then presenting some theory of operation, and finally discussing the specifications.

Figure 14 is a block diagram showing the major components of the polarimeter. The frequency-domain polarimeter consists of a receive-only dual-linearly polarized quad-ridged horn antenna built by Tecom Industries, Inc. It covers frequencies from 1.7 to 18.0 GHz. Depending on the frequency received, the gain of the antenna varies from 6 to 23 dB and the 3-dB beamwidth

Table 2—Output of Polarimeter for All Major Polarizations

| Polarization	3D Spatial Incidence on Antenna	Signal on single channel receiver	Frequency Spectrum	Output of Polarimeter
Horizontal →				$\|A\| = \|B\|$ A not in time-phase with B ($\varphi = 180°$)
Vertical ↑				$\|A\| = \|B\|$ A in time-phase with B ($\varphi = 0°$)
45° Slant ↗				$\|A\| \neq \|B\|$ Phase between A and B depends on how large A is. Therefore, φ is variable.
135° Slant ↖				$\|A\| \neq \|B\|$ Phase between A and B depends on how large B is. Therefore, φ is variable.
Right-hand Circular				At any instant in time : Two orthogonal components are equal (A = B). A is out-of-phase with B by 90°.
Left-hand Circular				At any instant in time : Two orthogonal components are equal (A = B). A is out-of-phase with B by -90° or 270°.
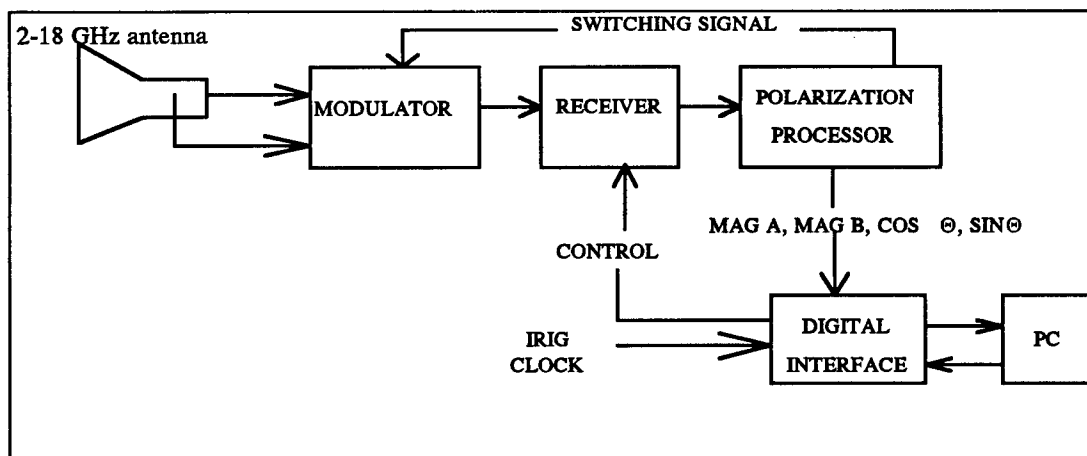
Fig. 14— System block diagram

varies from 67° to 6°. The outputs from the two antenna ports are fed to the superheterodyne receiver via a single channel. This is accomplished by switching between the two ports of the antenna at a 10 MHz rate. The IF output is processed to extract the polarization data which is sent to a digital processor which combines the data into dwell descriptors. These dwells are collected and stored by the computer. IRIG time is also read by the computer so that the data collected can be correlated with emitter signals.

4.1 User Input

Before data collection, commands to the receiver and data collection parameters are entered by the user via the system's computer. The following parameters are entered:

Setup Menu	Ranges
Frequency of emitter to be measured	2000-17750 MHz
RF Attenuation (Automatic or Manual)	0-70 dB / 10 dB steps
Threshold	0-63 dB / 1 dB steps
Data Display Mode	Average /Engineering /Hex /Off
Buffer size	16 or 64 pulses
Time of data collection	1 - 1500 s

The RF attenuation can be entered manually by the operator or it can be set automatically by the receiver. If set manually, the operator can observe the signal level while adjusting the gain of the receiver until a desired operating point is achieved. The desired operating point depends on the signal power of the emitter being measured. The attenuation may be set at a maximum of 70 dB in 10 dB steps. If the automatic mode is selected, the receiver reads the amplitude of the incoming signal and adjusts the RF attenuator in the RF section until the log amplifiers in the IF section are within their linear operating range. Despite the mode of operation chosen, this gain setting remains unchanged until the operator enters another value.

The threshold setting indicates the power level for detection of the signal over the noise level. For weak signals, the threshold should be set at a smaller value (12 dB) than for stronger signals where a 15 dB threshold setting would be sufficient. It is recommended that during operation the

attenuation should be set in the automatic mode and the threshold adjusted until the proper readings are received.

4.2 Receiver Tuning

The number of pulses actually collected during each 50 ms dwell depends on the PRF of the emitter. This information is sent from the computer (see Section 4.5) to the receiver controller as shown in Fig. 15. Here the receiver commands are decoded to

1. a 12-bit center frequency word - to correct the oscillator frequency that goes to Mixer B
2. a 3-bit attenuation word - to attenuate the incoming signal by a set value
3. a 12-bit YIG filter input - open loop command to tune the YIG filter
4. two ENABLE signals - to control the sampling switch and the calibration oscillator.
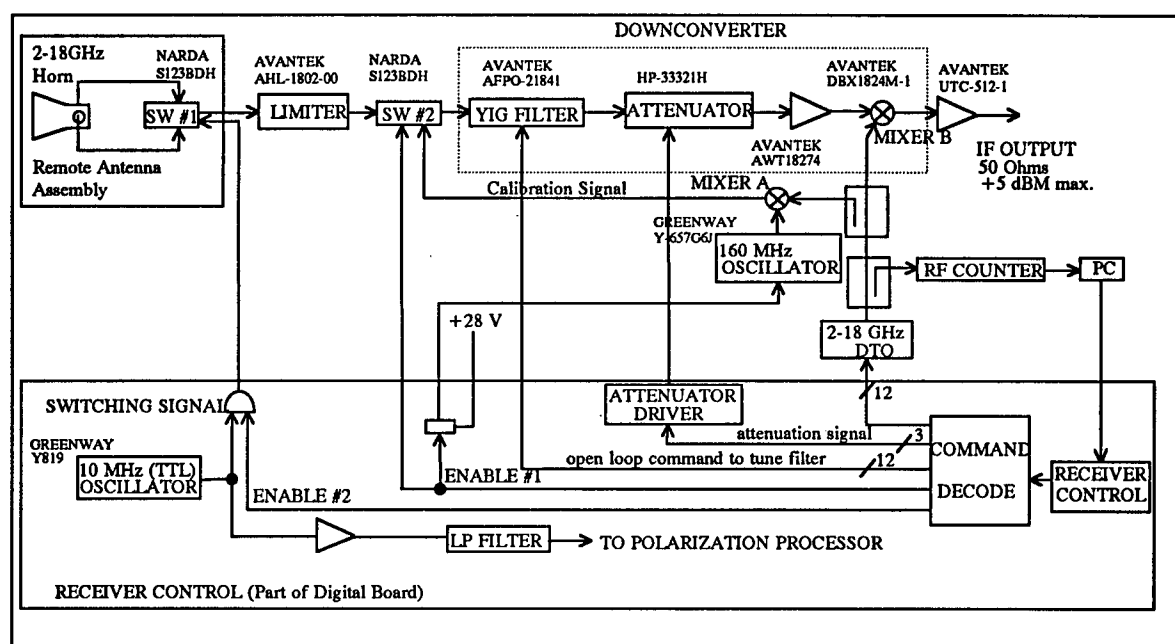

Fig. 15—Block diagram of RF section of polarimeter

When the user hits "enter" on the system's computer keyboard after setting the parameters mentioned in the previous section, the receiver frequency is tuned to the commanded frequency. The tuning process takes place in the RF section of the polarimeter, shown in Fig. 15. The following steps describe the frequency tuning process.

a. The computer reads the command frequency (f_{com}) from the set-up menu.
b. The computer offsets f_{com} by the IF frequency (160 MHz) to create the local oscillator (LO) frequency, converts it to a digital word, and sends it as a 12-bit frequency value to the digitally tuned oscillator (DTO). The LO frequency at this point becomes

$$f_{LO} = f_{com} - 160 \text{ MHz.}$$

c. A measurement of the oscillator frequency is made by the continuous wave (cw) RF counter to determine the tuning error.

d. The computer reads the frequency on the counter (f_{com} - 160) and if it is not within 2 MHz of the commanded frequency, it sends commands to the DTO to correct its frequency.

e. The YIG filter is tuned in 2 MHz steps to ±40 MHz about the commanded frequency, until a maximum signal level is observed at the IF output.

After the frequency of the receiver is tuned, the 40 MHz bandwidth YIG filter is calibrated. This procedure is done to center the YIG filter at the operating frequency. Therefore, during data collection, any signal within ± 20 MHz of the tuned frequency may be received. This feature of the polarimeter may cause unwanted pulses to be stored in the buffer when measuring several radar signals simultaneously having frequencies within 20 MHz of each other.

The following steps calibrate the filter.

a. The modulator in the remote antenna assembly is disabled. This is done by blocking the 10 MHz oscillator signal with the ENABLE #2 signal from the computer.

b. The calibration signal is enabled (ENABLE #1 signal) by placing +28 V on the 160 MHz oscillator (i.e., to power it up). This +28 V supply is used only during the calibration procedure.

c. The calibration signal is generated at the center of the RF band by mixing the LO frequency with the output of the 160 MHz oscillator (in Mixer A). The calibration signal is a coarse value of the commanded frequency.

d. This calibration signal is then injected in the receiver and is monitored by the computer as the filter is slewed. This is done by reading the amplitude of the received signal and applying the 10 dB RF attenuation until the signal is no longer saturated. The signal is then tested for a peak value by finding the two 3 dB points and centering between the two.

e. Calibration is complete when the peak value of the received signal is detected. The calibration signal is disabled by removing the +28 V from the 160 MHz oscillator to assure that no internally generated interference is created. Switch #2 is disabled by the same signal from the computer and therefore becomes a straight-through path.

When the tuning process of the filter is complete, the antenna modulator is enabled, the receiver input is reconnected to the antenna input, and the LO frequency is reduced by 5 MHz so that at the output of Mixer B, the "carrier" is at 165 MHz and the "lower sideband" is at 155 MHz.

4.3 Operation of the Polarimeter

When a signal enters the dual linearly polarized antenna, the orthogonal outputs (e.g., V or H) are sampled by a PIN Diode switch (Switch #1) whose switching signal is generated by a 10 MHz reference signal from the receiver controller. The switching process may form an "on/off" AM wave on the single channel, with modulation depending on the power of the signal received on the

two outputs. This signal is 100% amplitude modulated if and only if the received signal is 100% vertically or 100% horizontally polarized; it is 0% amplitude modulated if the signal received is a perfect 45° or 135° slant polarized wave. Since these ideal situations rarely occur, the signal received is almost never 100% or 0% amplitude modulated. Figure 16 is a representation of the amplitude modulated signal received by the polarimeter for an almost vertically polarized wave.
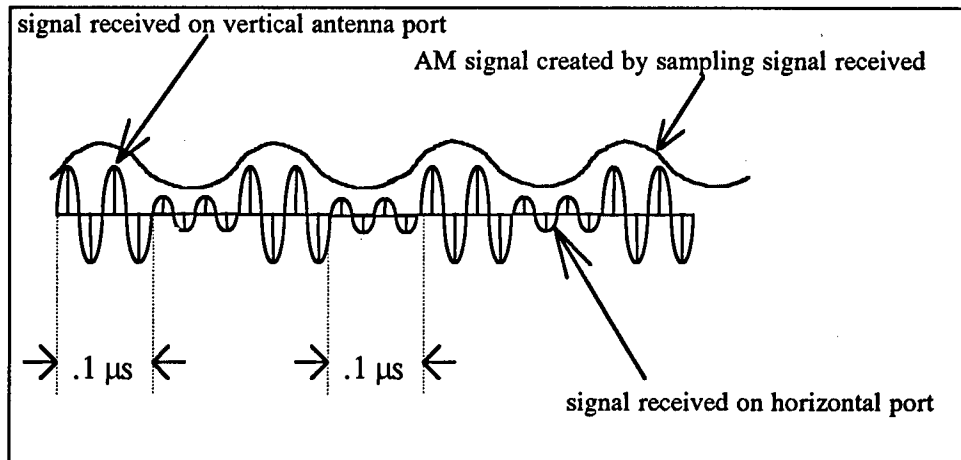

Fig. 16—Vertically polarized signal as received by a single channel polarimeter receiver

The receiver is protected with a 10 dBm limiter where any signal entering the receiver above this level is limited to 10 dBm. Switch #2 is not enabled at this time because it is only used for the tuning procedure. All of the signals received are then filtered through the 40 MHz bandwidth YIG filter.

After the RF signal is amplified with a low-noise amplifier, it is heterodyned (i.e., mixed) in a double-balanced mixer (Mixer B) with the LO frequency from the DTO to establish the intermediate frequency (IF). The IF signal, the difference in frequency of the received emitter signal and the LO signal, is nominally 160 MHz. The signal is amplified again with an amplifier that operates at an IF output centered at 160 MHz and is sent to the IF processor of the polarimeter.

4.4 IF Processor Section

Upon entering the IF section, shown in Fig. 17, the carrier (*B* signal) is at 165 MHz and the lower sideband (*A* signal) is at 155 MHz. In the IF processor, the incoming signal is split into two paths with a power divider. Each path contains a 5 MHz bandwidth filter, one centered at 165 MHz and the other centered at 155 MHz. The 165 MHz filter extracts the carrier component (*B* signal) from the signal and the 155 MHz filter extracts the sideband (*A* signal) component.

The next step is to convert the carrier and sideband signals to a measurable representation of the 45° and 135° slant components of the measured electromagnetic wave. This 45° slant component is called vector *B* and the 135° component is designated as vector *A*. The two channels are factory balanced so that equal magnitudes are produced when vertical and horizontal polarizations are received.
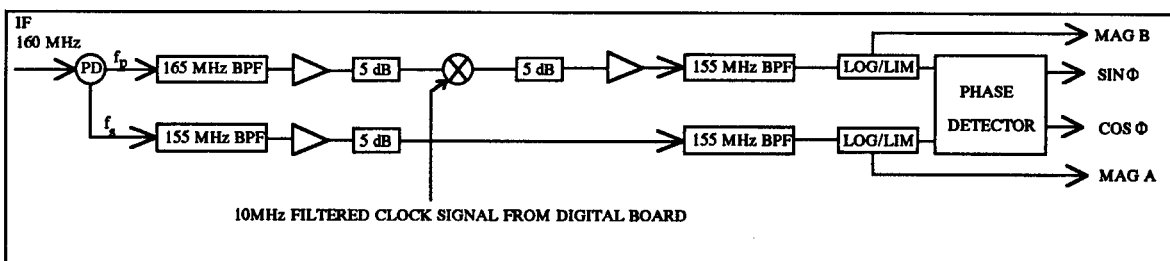
Fig. 17—Block diagram of IF section of polarimeter

The carrier frequency signal in the IF section is coherently beat down from 165 MHz to 155 MHz (the sideband frequency). This sets the outputs from the IF section to the same frequency allowing the relative phase between them to be measured. Both signals are then filtered at 155 MHz and fed to log/limiters. The logarithmic outputs from the IF section provide the magnitudes of the 45° and 135° slant components and the limiter outputs are fed to a phase detector where full I and Q processing is done, providing a quantified polarization measurement. The next stage is the digital processing.

4.5 Digital Processor Section

The magnitudes of the 45° and 135° slant components and the I and Q phase components are converted to 8-bit words in this section of the polarimeter, shown in Fig. 18. There are 2^n possible values for an 8-bit word ($2^8 = 256$), which provides the following resolutions for the polarization measurements:

Phase Resolution $= 360° / 256 = 1.4°$
Amplitude Resolution $= 60$ dB of Dynamic Range $/ 256 = 0.23$ dB

The time-of-arrival (TOA) counter is clocked at a 20 MHz rate. Therefore, the time difference from bit to bit of the 16-bit time-of-intercept (TOI) output from the counter is 0.05 µs. This implies that the maximum time of intercept on the clock is

$$\text{TOI} = 2^{16} * 0.05 \ \mu s = 65,536 * 0.05 \ \mu s = 3,276.8 \ \mu s.$$

In the output data from the polarimeter, the TOA data are time measured with reference to this clock. For example, a pulse received at 3,400 µs with reference to this clock will be recorded by the polarimeter with a 123.2 µs TOA (i.e., 3,400 µs − 3,276.8 µs). These resolutions can be improved by choosing analog-to-digital converters with a larger number of bits.

How the Pulse is Sampled

The Leading Edge (LE) Detect Circuit in the digital section samples the pulse. This is done by duplicating the pulse and delaying it by 50 ns. When the pulse is above the noise floor by the threshold commanded by the operator, the digitizing process begins. When the pulse crosses over the leading edge of the duplicated pulse, as shown in Fig. 19, an amplitude measurement is made and recorded. Only one amplitude measurement of each pulse is made. Additional hardware and different analog-to-digital converters would be required to sample the pulse more than once.
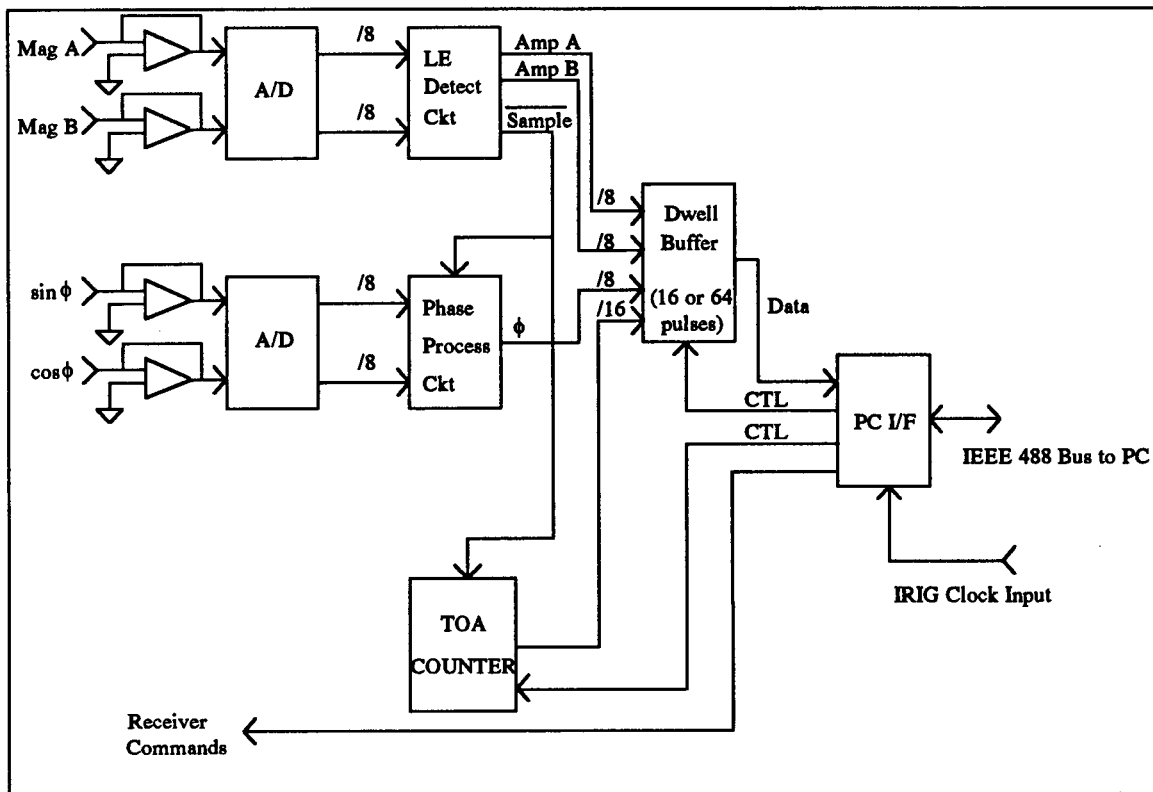
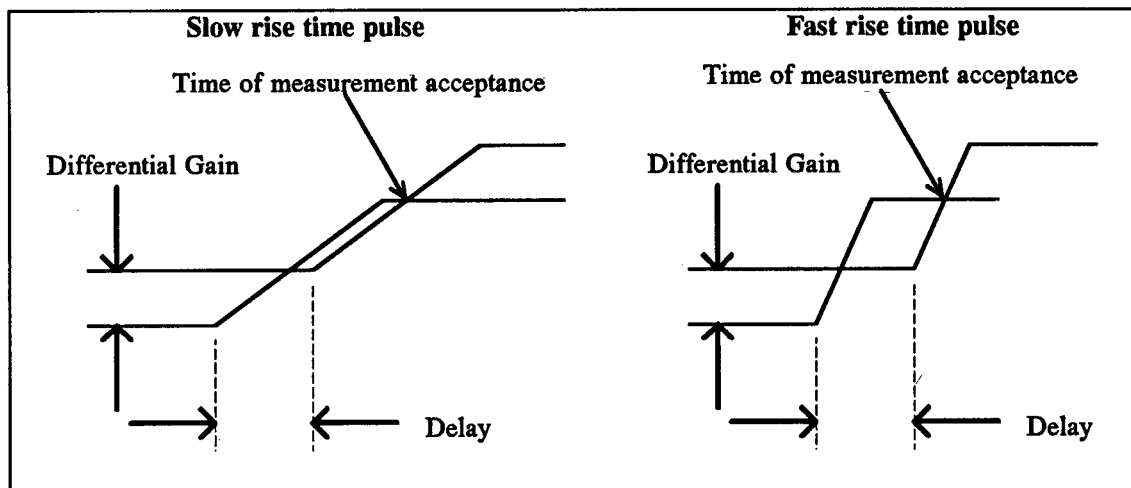Fig. 18—Block diagram of digital section of polarimeter

Fig. 19—Method used by polarimeter to sample a pulse

How Phase is Calculated

When the sampled pulse crosses over its duplicate in the sampling process described above, an enable signal is created that tells the Phase Process Circuit to calculate the phase at the time the cross-over occurs. The phase is calculated by

$$\text{Phase} = \arctan(\sin\phi \, / \cos\phi).$$

In addition, the TOA Counter, which is a wrap-around clock intended to operate for the amount of time commanded by the operator, is enabled by the same signal to record the time on the clock at which the amplitude and phase recordings are made. This time is useful in determining the interval between received pulses (i.e., the PRI of the emitter).

The amplitude of the 45° and 135° slant components (i.e., B and A), the phase between these two components, and the TOA of the pulse is sent to a buffer whose size is determined by the commanded value given by the operator. The maximum size of the buffer is 64 pulses. Even though it is not necessary for proper operation of the polarimeter, the pulses are appended with the IRIG time to form a pulse dwell descriptor. This descriptor is collected by and stored in the system's computer.

4.6 Specifications

Table 3 lists the specifications of the polarimeter. The sensitivity of the system is at -85 dBm because of the antenna used. The antenna is a dual-linearly polarized quad-ridged horn with a gain varying from 6 to 23 dB and a 3-dB beamwidth varying from 67° to 6° depending on the frequency of the signal it is receiving (1.7 to 18 GHz). An improved sensitivity would be seen with an antenna whose gain was higher.

The 10 MHz oscillator in the polarimeter, used for switching the dual-polarized antenna, allows measurements on pulses as narrow as 100 ns (1/100 ns = 10 MHz). However, the measurements on a pulsewidth this small look "flaky" because the bandwidth of a 100 ns pulse is wide enough to make the carrier and sideband frequency components interfere with one another. If the sampling rate were increased, the signals would reside further apart and no aliasing distortion would be present. Minor changes would be required to the polarimeter to measure pulses that are less than 100 ns wide. For example, if a 50 ns pulse is to be measured, an oscillator sampling at a 40 MHz rate (i.e., 2*BW = 2*(1/50 ns) = 2*20 MHz) would satisfy this requirement.

The minimum PRI value is determined by the throughput allowed by the analog-to-digital converters in the polarimeter. The speed of the converters allow for a maximum of 200 kilo pulses to be passed through every second. This allows for a minimum of 5 μs between each pulse (1/200 kilo pulses per second = 5 μs per pulse) and hence, a 5 μs minimum PRI.

The accuracy of the polarimeter was determined through chamber tests where the amplitude measurements were within 1 dB of the expected value and the phase was within 10° of the expected phase of the polarization being measured.

4.7 Polarimeter Output Data

The output of the polarimeter gives the amplitude of the 45° slant component of the electromagnetic wave, the 135° slant component of the same wave, and the time-phase difference between them. The plots in this report include three parameters: the power magnitude of the signals received, the difference of the magnitudes of the two polarization components (i.e., the signals at the carrier and sideband frequencies), and the time-phase difference between these two magnitudes.

Table 3—Specifications of Polarimeter

Parameter	Value
Type	Single channel, frequency domain
Frequency range	2 to 18 GHz
Sensitivity	-85 dBm
Instantaneous dynamic range	60 dB
Pulsewidth range	0.2 to 10 μs
PRI range	5.0 μs to 10 ms
TOI range	0 to 3.27 ms
Throughput	200 Kpps
Polarization measurement accuracy	1 dB amplitude
	10° phase
Polarization measurement resolution	0.23 dB amplitude
	1.4° phase
TOI resolution	0.05 μs
Parameters recorded internally	TOI in μs
	Relative 45° left-slant polarization component in dB
	Relative 45° right-slant polarization component in dB
	Phase angle between components in degrees
	IRIG (B): hundredths of second, tenths of second, seconds, minutes, hours
Internal data recording resolution	8 bits
Internal data recording medium	120 Mbyte hard drive + high density 3.5 in. floppy disk
Prime power for computer	110 VAC, single phase, 60 Hz, 60 watts
Power for entire system	110 VAC, single phase, 60 Hz, 250 watts
Antenna Specifications	
Gain	6 to 23 dBi
Nominal 3 dB beamwidth	67° to 6°
CW power	5 watts
Isolation	20 dB
Impedance	50 Ω

The graphs in this report plot this polarization information for each pulse measured. This plotting procedure was chosen, as opposed to averaging the data over some number of pulses, because these navigation radars were rotating so fast (2.5 s per revolution) that if the data were averaged, too many angles of rotation and, hence, a wide range of signal power, would be included in each average.

As presented in the Appendix, the amplitudes of these signals are equal only if a vertical, horizontal, right-hand circular, or left-hand circular polarization wave is received. They are not equal if a 45° or a 135° polarization signal is received. Instead of showing each amplitude separately, the difference between the amplitudes of the components is shown. Therefore, the difference-in-amplitude graph should be close to zero if a vertical, horizontal, right-hand circular, or left-hand circular polarized pulse is received and of noticeable difference (10-15 dB) for a 45° or 135° polarized pulse. The time-phase between the 45° and 135° vector components is presented as measured by the polarimeter described in Section 3. Figure 20 shows what values to expect on the output plots in this report for the polarizations measured.
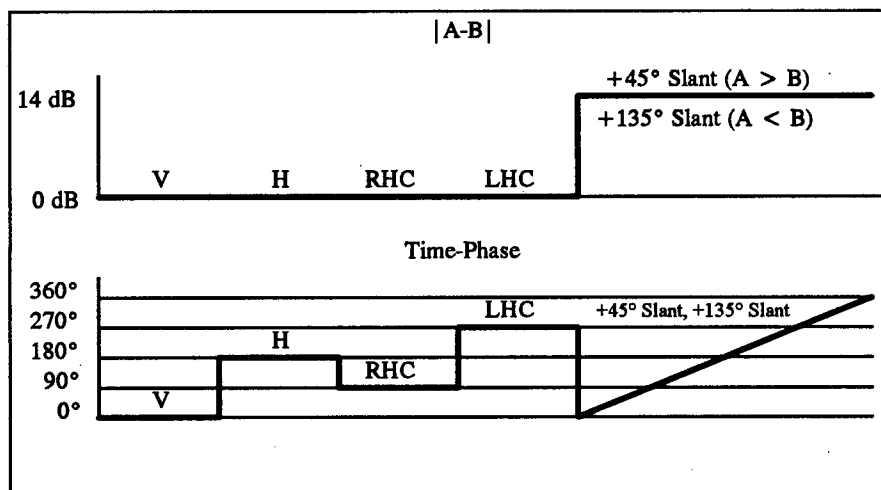
Fig. 20—Representation of measured polarization by Frequency Domain Polarimeter

The polarimeter collects pulses for 50 ms and processes them for another 50 ms. Therefore, during the 50 ms processing time the polarimeter is not collecting data, and, in the meantime, the radar being measured continues to rotate. This may sometimes cause the polarimeter to miss data from the mainbeam of the antenna when the rotation rate is fast (2.5 s per revolution). The plots of the polarimeter data presented in this report include the 50 ms processing time, which is shown by the straight line connecting the last point of the data collected prior to the processing gap to the first point of the data collected after the processing gap.

5. RADAR ANTENNA CHARACTERISTIC TEST

A field test was conducted in August 1992 at the Naval Air Warfare Center - Aircraft Division (NAWC-AD), Patuxent River, MD to evaluate the antenna polarization characteristics of various navigation radars. The intent of this test was to measure and analyze antenna polarization characteristics to evaluate whether or not the information can be used for NCTR. The three specific objectives of the test and the approach used to accomplish them are discussed in Sections 5.1 and 5.2. The characteristics of the navigation radars measured are provided in Section 5.3 and the theory of the polarization characteristics of these emitters is explained in Section 5.4. The results for each objective of the test are presented and discussed in Section 5.5.

In the remainder of this report, "types" refers to navigation radars (as opposed to, for example, search radars); "models" refers to different radar designs (e.g., the FR602D and the FR8100).

5.1 Test Objectives

Phase I: Scan-to-Scan Antenna Characterization

The first objective of this test was to show that two not necessarily consecutive revolutions of the same radar unit are similar in mainlobe and sidelobe polarization characteristics. The intent was to determine if a radar could be identified with antenna polarization characteristics from a single scan.

Phase II: Position-to-Position Antenna Characterization

The second phase of this test compared the mainlobe and sidelobe antenna characteristics of the same radar unit radiating from three different geographical positions. The objective was to see whether or not the polarization characteristics of an antenna are the same when measured from different locations having approximately the same multipath environment (i.e., over water but with different background reflections).

Phase III: Radar-to-Radar Antenna Characterization

The objective of this phase of the test was to see if two different radar models can be distinguished by analyzing their antenna polarization characteristics. First, the intent was to investigate any similarities and/or differences in the polarization characteristics between two similar antennas (i.e., same model but with different serial numbers), each measured individually at the same location. The second objective of this phase was to evaluate the characteristics from two different antenna models, whether in the same location or not, and determine if and how they are different.

5.2 Approach

The approach used to determine if antenna polarization information can be used to identify radars was to measure the antenna polarization of two navigation radars with the same type of antenna and one navigation radar whose antenna is different from the other two. The measurements were done with the navigation radars on boats located at different locations in the Chesapeake Bay and with the polarimeter on a stationary land site. Each radar was measured independently (i.e., one radar was turned on at a single time) and the antennas were rotating constantly.

The following three positions were chosen for locating the vessels during the measurements.

Position 1 : 145° from due North and 2.6 miles from test site (i.e., polarimeter location)
Position 2 : 105° from due North and 3.0 miles from test site (i.e., polarimeter location)
Position 3 : 50° from due North and 2.5 miles from test site (i.e., polarimeter location).

Figure 21 is a map of the area where the tests were performed, showing the three locations for the boats and the location of the polarimeter test equipment. The range from the radars to the polarimeter had to be less than or equal to three miles because of the live firing beyond three miles from the test site. For each data collection, the antenna of the polarimeter was turned to point towards the boat. Figure 22 shows the polarimeter as it was set up for this test.

No IRIG time code generator was available and, therefore, the files generated by the polarimeter, which are usually named after the starting IRIG time of data collection, were named manually by the user. The name of each file contains the month, date, hour, and minute at which the data was collected. For example, a file named 8260720.dat indicates that the data was collected on August 26th at 7:20 am.

5.3 Radar Characteristics

The two Model A navigation radars measured were the Furuno FR602D, pictured in Fig. 23. Each radar was mounted on a different boat; one FR602D was on the *Septar 06*, shown in Fig. 24,
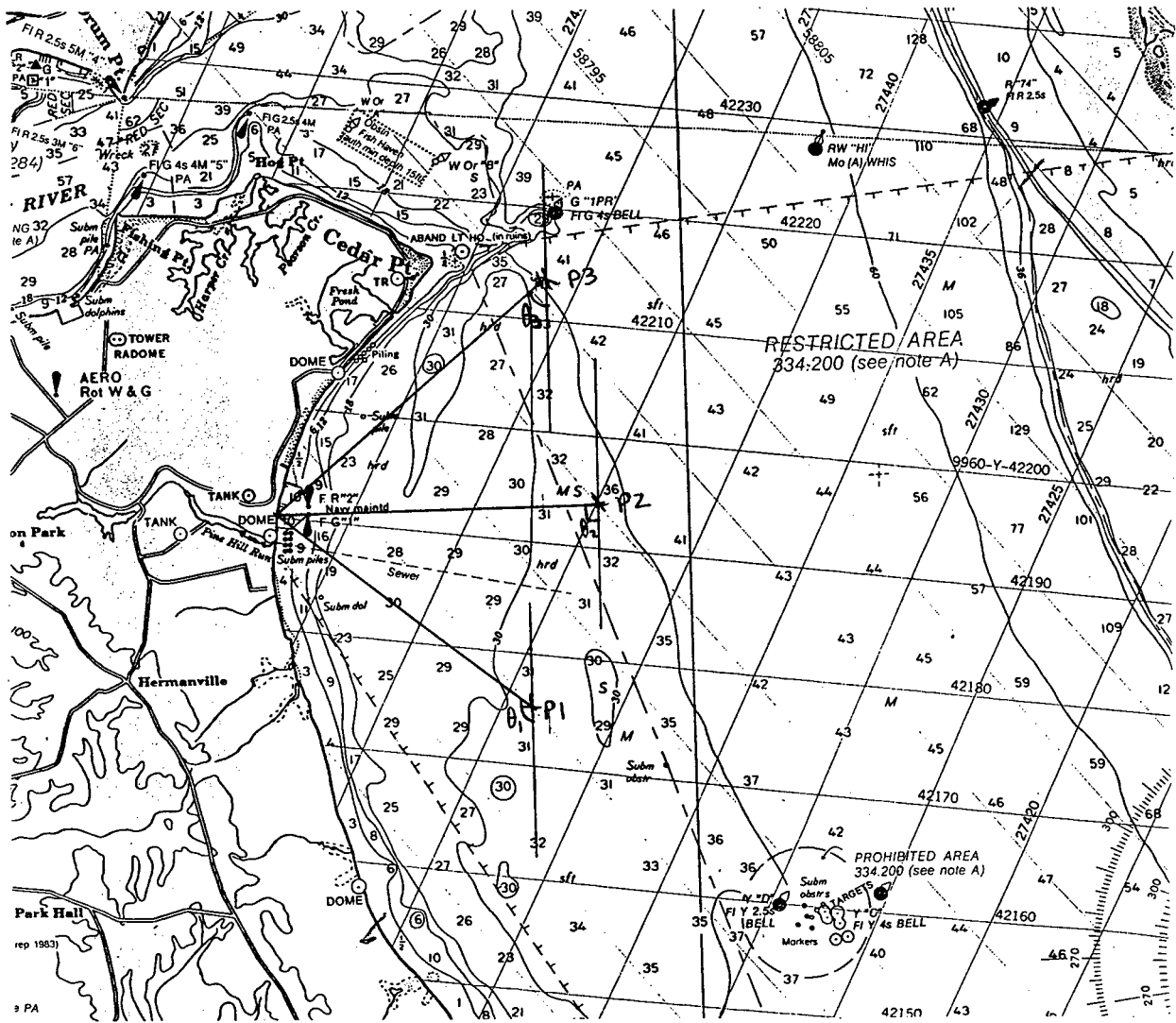
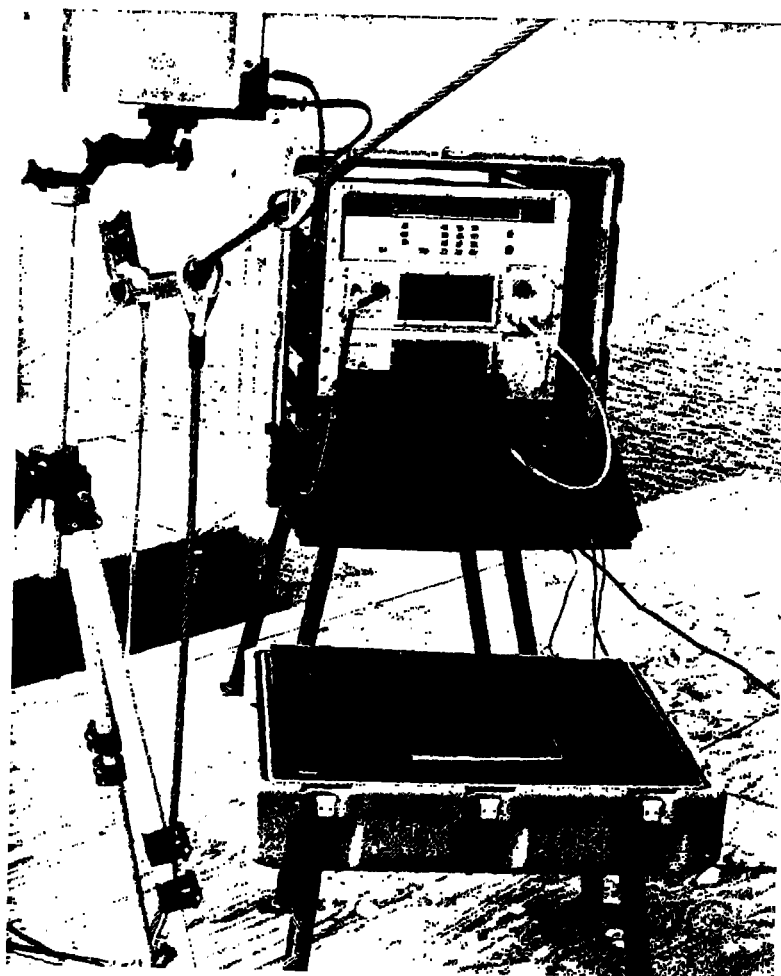Fig. 21—Map of test site showing positions of boats
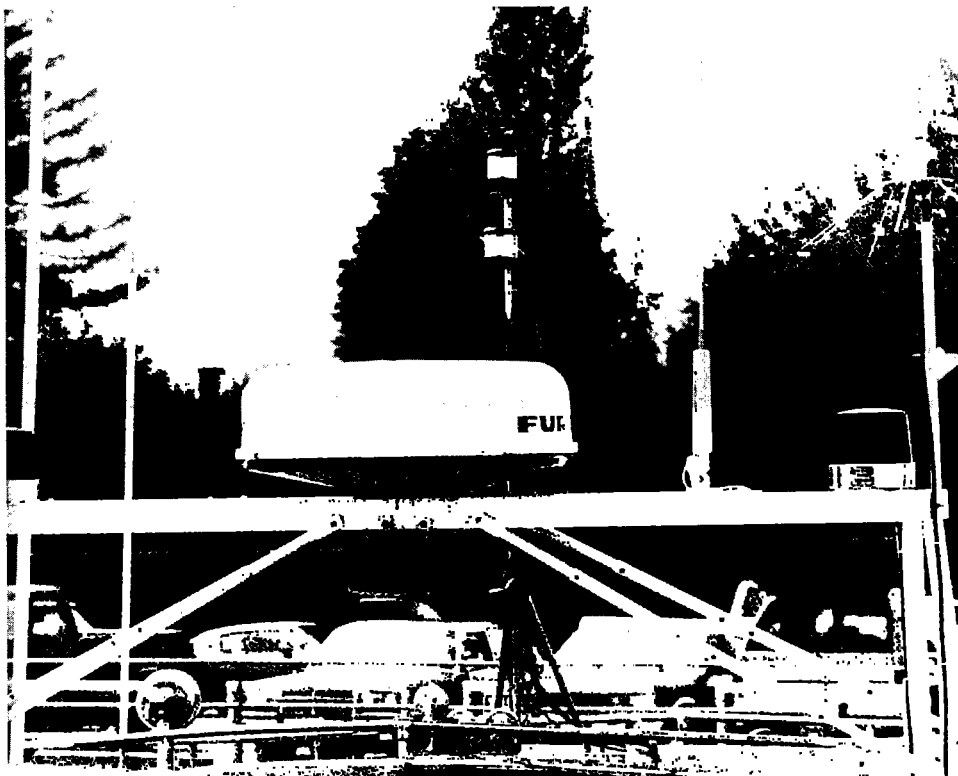
Fig. 22—Polarimeter setup for field test

Fig. 23—Furono FR602D navigation radar setup

Fig. 24—The FR602D aboard the *Septar 06*

and the other was on the *Prince*, shown in Fig. 25. The Model B radar was the Furuno 8100 navigation radar, shown in Fig. 26. This radar was mounted on the *Transporter*, as shown in Fig. 27. Table 4 lists the characteristics of the radars measured.

Several differences between these two radar models are important to polarization measurements. The FR602D radar has a center-fed waveguide enclosed in a radome, whereas the FR8100 radar is an open radome antenna whose waveguide is fed from the end. The FR602D has a smaller radiator (80 cm) than does the FR8100 (200 cm), which as we have seen from the theory possesses a difference in copolarization-to-cross-polarization ratio in the sidelobes. The beamwidth of the FR8100 antenna is smaller in both the horizontal and the vertical directions, giving this radar a longer detection range (72 nmi).

5.4 Theory of Operation of Edge-slot Waveguides

In the design of waveguide-fed slotted arrays, three types of slots can be made in the waveguide: longitudinal slots in the broad wall of the waveguide; centered and slanted slots in the broad wall of the waveguide; and slanted slots in the narrow wall of the waveguide. Figure 28 shows these three slot configurations.

The longitudinal slots are used to obtain a transmit polarization that is perpendicular to the long axis of the waveguide; the edge slots are used to transmit an electromagnetic field whose polarization is parallel to the long axis of the waveguide. This happens because the radiation pattern from a slot in a waveguide is the same as a half-wavelength dipole, rotated by 90°. Figure 29 shows an edge-slot array with slots separated by one-half of a wavelength and its dipole representation. The intensity and polarity of the transmitted waveform depends on the number and the direction of tilt of the slots [7].

The copolarized and the cross-polarized components of the electric field radiated from a dipole are given by the following equations:

$$E_{co-pol} = E\vartheta \cos\vartheta N'$$

$$E_{x-pol} = E\vartheta \sin\vartheta N'$$

where

$$E\vartheta = \frac{\cos\left(\frac{2\pi H}{\lambda}\sin\vartheta\right) - \cos\left(\frac{2\pi H}{\lambda}\right)}{\cos\vartheta}$$

ϑ = angle off boresight

N = number of slots in array

σ = spacing of successive elements (degrees)

H = length of each dipole

$$N' = \left[\frac{\sin\left(N\frac{s}{2}\sin\vartheta\right)}{\sin\left(\frac{s}{2}\sin\vartheta\right)} \right]$$
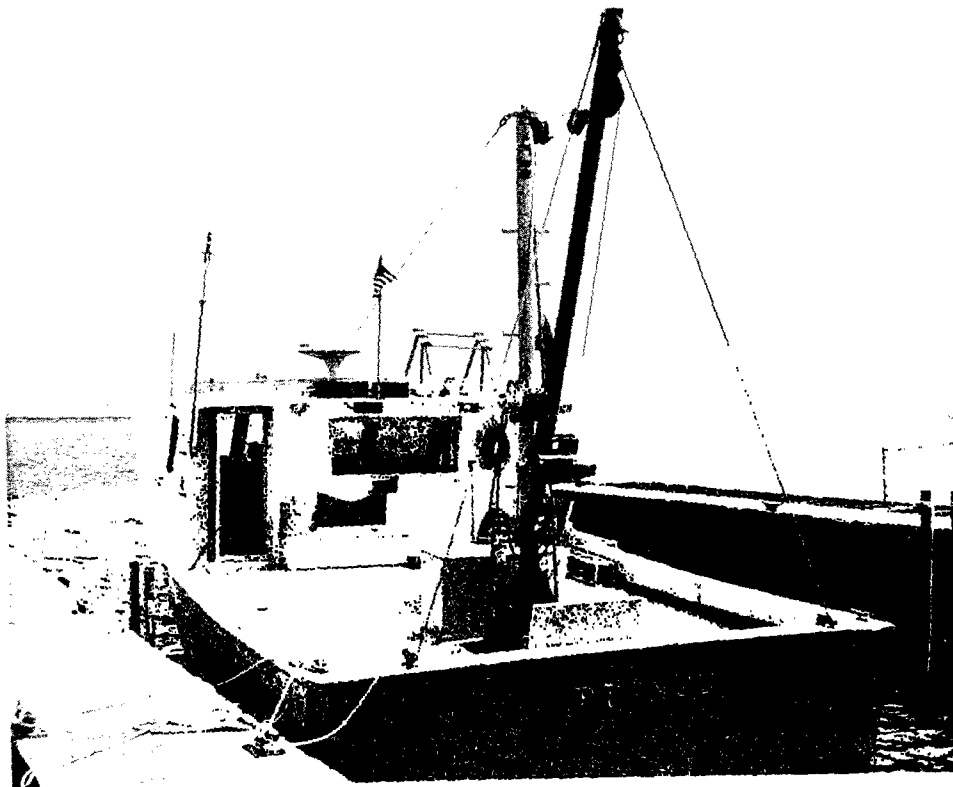
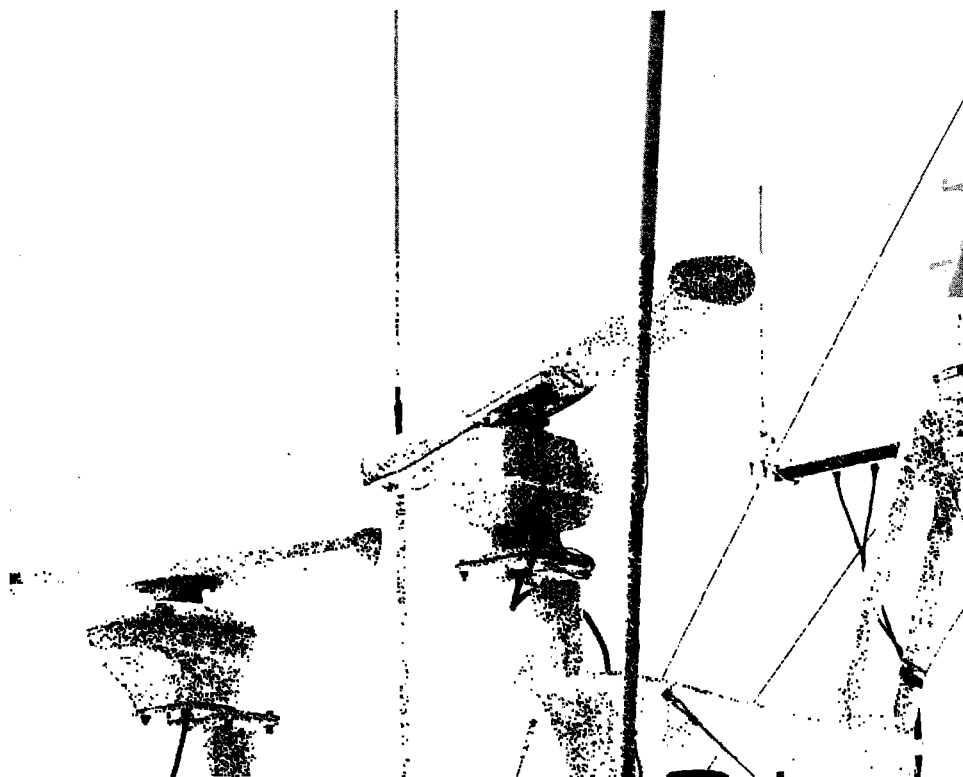Fig. 25—The FR602D radar aboard the *Prince*

Fig. 26—FR8100 navigation radar setup

Fig. 27—FR8100 radar aboard the *Transporter*

Table 4—Characteristics of Furuno 602D and Furuno 8100 Navigation Radars

Radar Characteristic	FR602D	FR8100
Scanner Unit		
Radiator	Center-fed slotted waveguide array (housed in radome)	End-fed slotted waveguide array (open radome)
Radiator length (cm/ft)	80 / 2.6 (dome) 20" (array)	200 / 6.5
Horizontal BW (°)	2.7	1.23
Vertical BW (°)	25	20
Sidelobe attenuation	23 dB (< ±20° of mainlobe) 26 dB (> ±20° of mainlobe)	28 dB (< ±10° of mainlobe) 32 dB (> ±10° of mainlobe)
Polarization	Horizontal	Horizontal
Rate of antenna rotation with no wind load	24 rpm	24 rpm
Transceiver Unit		
Frequency (MHz)	9410 ± 30 (specification) 9400 (measured)	9410 ± 30 (specification) 9419 (measured)
Peak output power (kW)	3	10
Maximum range (nmi)	32	72
Pulse repetition rate (Hz)	3360 (range < 2 nmi) 840 (2 nmi < range < 32 nmi)	2100 (range < 3 nmi) 1200 (3 nmi < range < 24 nmi) 600 (6 nmi < range < 72 nmi)
Pulse length (µs)	0.08 (range < 2 nmi) 0.6 (2 nmi < range < 32 nmi)	0.08 (range < 1.5 nmi) 0.3 (1.5 nmi < range < 3 nmi) 0.6 (3 nmi < range < 24 nmi) 1.2 (6 nmi < range < 72 nmi)

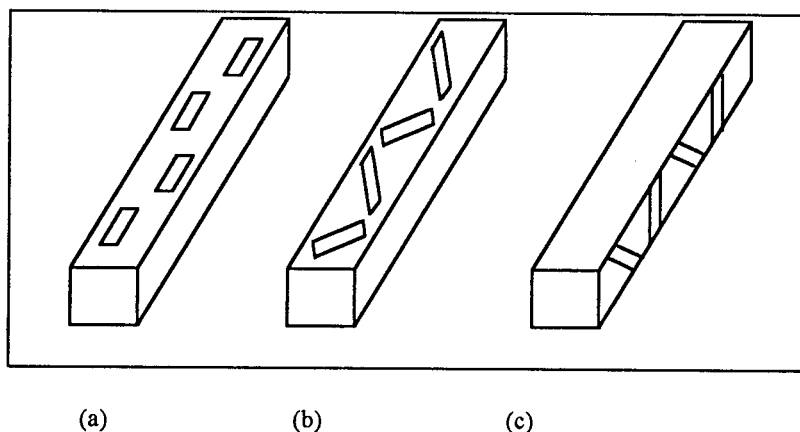(a)   (b)   (c)

Fig. 28 —Slotted waveguide configurations: (a) longitudinal broad wall slots, (b) centered slanted broad wall slots, and (c) slanted narrow wall (edge) slots
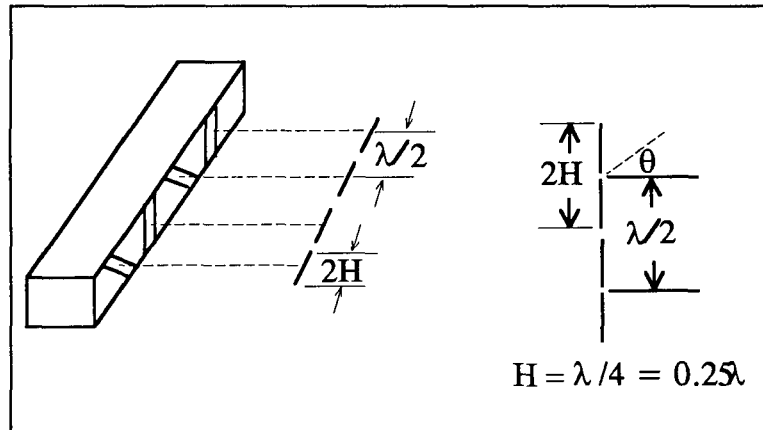
$$H = \lambda / 4 = 0.25\lambda$$

Fig. 29—Electric dipole representation of a slotted waveguide

Figure 30 plots the co-and cross-polarization components of a single dipole and a 100-dipole array between ± 90° off the perpendicular direction to the dipole (θ = ± 90°). These patterns are identical on both sides of an ideal dipole. These plots assume negligible mutual coupling between individual dipoles. In both cases, the copolarization component is maximum at boresight and the cross-polarization component is either zero or very small relative to the copolarization component. The ratio of the copolarization to cross-polarization at the mainbeam is maximum, giving the most accurate polarization measurement. As the angle off boresight, θ, increases, the copolarization-to-cross-polarization ratio decreases, which changes the polarization of the wave.

For a horizontally polarized slotted waveguide array, vertical slots would be required in the waveguide. Because there is no cross-polarization component of the wave in the principal plane, the wave is completely copolarized. As the angle off boresight increases, however, a cross-polarized component exists, which changes the cross-polarized-to-copolarized ratio and, hence, changes the polarization of the wave [8]. For example, when the cross-polarization component equals the copolarization component, the polarization of the wave would be 45° slanted. Note in the plots of Fig. 30 that at some points the copolarized component is zero and the cross-polarized component is not. At these points, the antenna would appear to be cross-polarized (i.e., vertically polarized).

These patterns look the same on both sides of a dipole. However, the waveguides of these navigation radars are slotted on only one side and therefore, the pattern becomes obstructed because of the structure of the radar. It is unlikely that the polarization characteristics of the backlobes of any navigation radar are the same as the characteristics in the front lobes.

The waveguides may be standing-wave fed, where the slots are separated by one-half of the waveguide's wavelength, or they may be travelling-wave fed, meaning that the slots are separated by some wavelength other than one-half. If the slots are separated by one-half the wavelength of the waveguide, as shown in Fig. 29, then the E-fields in the slots have a common phase and an arbitrary amplitude distribution.

The radars measured in this test are single waveguides with slanted edge-slots separated by approximately 2 cm. The FR602D radar has a 20-in. radiating array (51 cm) and the FR8100 radar has a 6.5-ft array (198 cm). Therefore, there are approximately 25 slots in the FR602D radar waveguide and approximately 100 slots in the FR8100 radar waveguide.
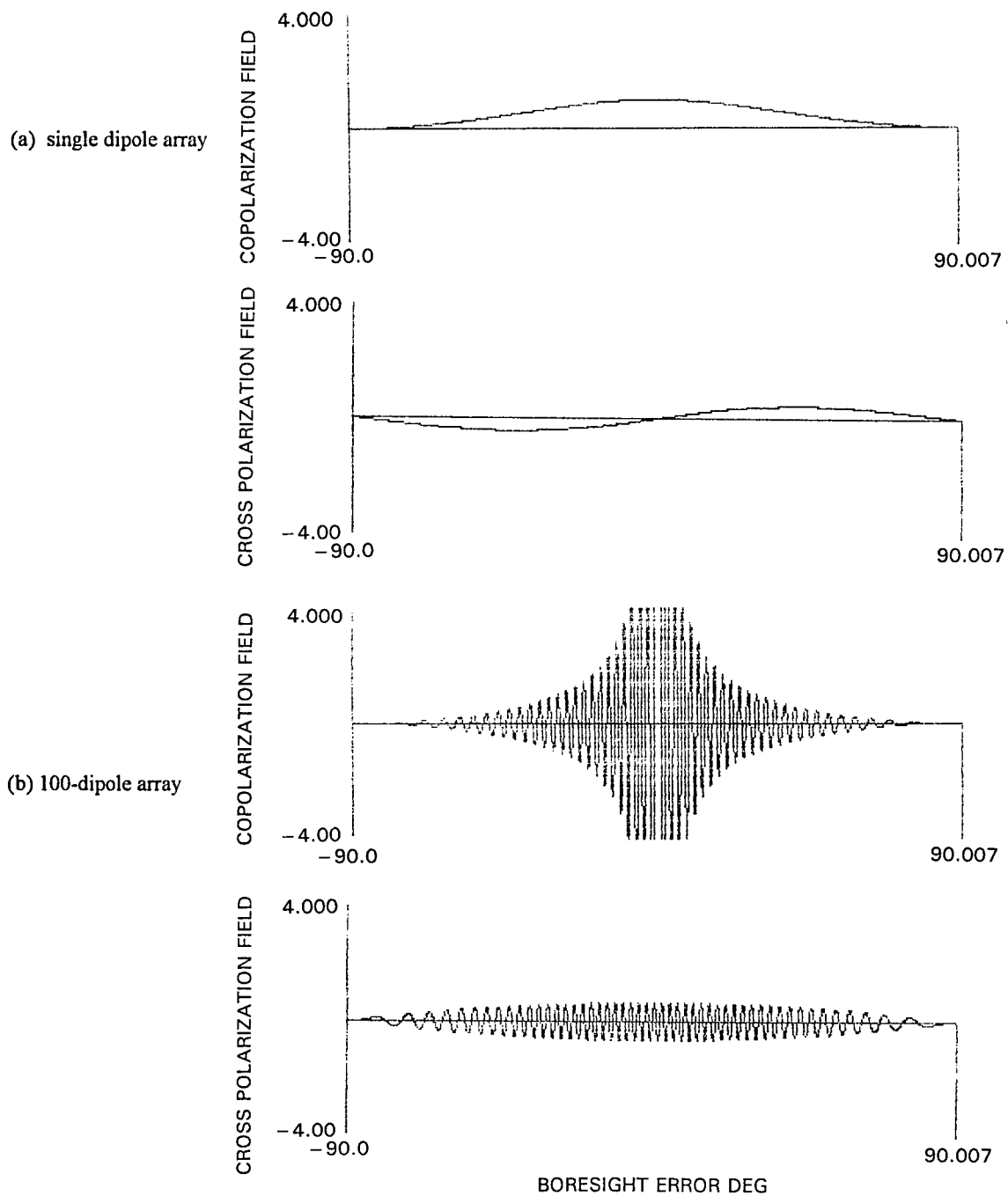
(a) single dipole array

(b) 100-dipole array

BORESIGHT ERROR DEG

Fig. 30— Copolarization and cross-polarization components of (a) single and (b) 100-dipole arrays

5.5 Results

Before presenting the antenna polarization data collected from the navigation radars, an explanation of the data format is given. While analyzing some of the data, it was observed from the TOA data that there appeared to be an interfering signal. To properly represent the polarization characteristics of the radars measured, a sorting routine was implemented on the data to extract any interfering signals and plot only the pulses from the radar of interest. This routine sorted the data with the PRI of the radar by finding the TOAs separated by the PRI value. Since the exact PRI was not measured, an error factor of Δt was added in. The following equation best describes the logic used to sort the data.

$$TOA_{x+n} = TOA_x + PRI \pm \Delta t$$

where

> TOA is the time of arrival recorded in polarimeter data files
> X is the pulse number
> n is 1,2,.....
> Δt is the error time factor

Figure 31 is a sample of a data file from the FR602D radar with an interfering signal. The second column of data is the time-of-arrival of the pulses recorded as measured by the internal clock, the third and fourth columns are the 45° and 135° slant polarization components (Amp A and Amp B) of the EM wave, respectively, and the last column is the time-phase difference between Amp A and Amp B (columns three and four). Note from the TOA data of Fig. 31 that some of the pulses are separated by approximately 1200 μs (the PRI of the FR602D radar) and the pulses in between them are separated by 1561 μs (the PRI of the interfering emitter). The difference-in-magnitude data (difference between magnitude A and magnitude B) of these pulses is approximately 2 to 5 dB, whereas the same data for the interfering pulses is approximately 8 to 10 dB. The time-phases of the FR602D radar pulses are in the vicinity of 180° (i.e., horizontal polarization); the time-phase data of the interfering signals are in the vicinity of 0° (i.e., vertical polarization). The x's in Fig. 31 indicate the pulses selected by the sorting routine for the FR602D radar.

An example showing the before-sorting-routine data and the after-sorting-routine data is shown in Fig. 32 (a) and (b), respectively. This figure shows how the sorting routine eliminated the pulses from the interfering signal.

Phase I: Scan-to-Scan Antenna Characteristic Test

Procedures

The purpose of this section of the test was to investigate any similarities and/or differences in the antenna polarization characteristics between scans of a radar. Each vessel was positioned in each of the three designated locations, and while in those positions, their radars were allowed to rotate at a constant rate of 24 rpm. Six sets of data were collected for each radar in each of the three fixed positions. Three of the six sets collected 12 s of data, equivalent to approximately 5 revolutions of the radar

$$(24 \text{ rev/1 min}) \times (1 \text{ min/60 s}) \times 12 \text{ s} = 4.8 \text{ rev},$$

	TOA (ms)	Amp A (dB)	Amp B (dB)	Phase (deg)	
0	472.85	38.48	46.10	7.03	
1	970.35	42.67	50.67	189.84	
2	2034.50	36.95	45.71	7.03	*
2	2034.50	36.95	45.71	7.03	
3	2159.95	43.43	50.67	189.84	X
4	71.85	44.95	50.67	195.47	X
5	319.30	36.57	44.95	12.66	
6	1262.35	46.10	50.67	198.28	X
7	1881.00	38.86	46.48	12.66	
8	2451.95	45.71	49.14	202.50	X
9	165.80	35.05	45.33	8.44	
10	364.75	48.00	51.05	202.50	X
11	1554.35	49.52	51.05	206.72	X
12	1727.45	38.10	44.95	12.66	
13	2743.95	46.86	48.76	205.31	X
14	12.30	35.43	45.33	5.62	
15	656.75	49.14	49.90	208.12	X
16	1573.95	38.86	46.48	8.44	
17	1845.45	46.48	46.86	206.72	X
18	3036.55	49.52	49.90	208.12	X
19	3135.60	38.10	45.71	4.22	
20	948.85	54.10	52.19	205.31	X
21	1420.40	36.57	45.33	16.88	
22	2138.45	55.62	53.33	210.94	X
23	2982.10	39.24	46.48	12.66	
24	50.30	53.71	50.67	212.34	X
25	1240.80	50.67	44.19	210.94	X
26	1266.90	37.71	45.33	9.84	
27	2430.45	54.48	52.57	212.34	X
28	2828.55	39.24	45.33	14.06	
29	342.35	55.24	53.33	212.34	X
30	1113.40	37.71	46.10	7.03	
31	1531.60	57.90	54.10	217.97	X
32	2675.05	38.48	46.86	14.06	
33	2722.45	55.24	52.19	216.56	X
34	635.25	54.48	51.05	225.00	X
35	959.90	38.86	45.33	12.66	
36	1824.85	54.86	50.67	226.41	X
37	2521.50	35.05	44.95	4.22	
38	3014.50	57.14	50.67	237.66	X
39	806.35	37.33	44.19	14.06	
40	927.30	57.14	50.67	240.47	X
41	2117.50	57.14	49.90	244.69	X
42	2368.00	36.95	45.33	7.03	
43	29.65	51.43	43.43	244.69	X
44	652.85	39.62	45.71	11.25	
45	1219.25	50.29	44.19	247.50	X
46	2214.50	37.33	45.33	5.62	
47	2408.95	54.86	43.81	257.34	X
48	321.75	53.33	44.19	272.81	X
49	499.35	38.48	46.10	5.62	
50	1511.35	50.29	42.67	286.88	X
51	2061.00	38.10	45.71	19.69	
52	2700.95	46.86	42.67	329.06	X
53	345.80	37.33	45.71	7.03	
54	613.45	43.05	44.19	345.94	X

The left margin contains bracketed annotations of "1,200 μs" spanning pairs of rows (between rows 4–20).

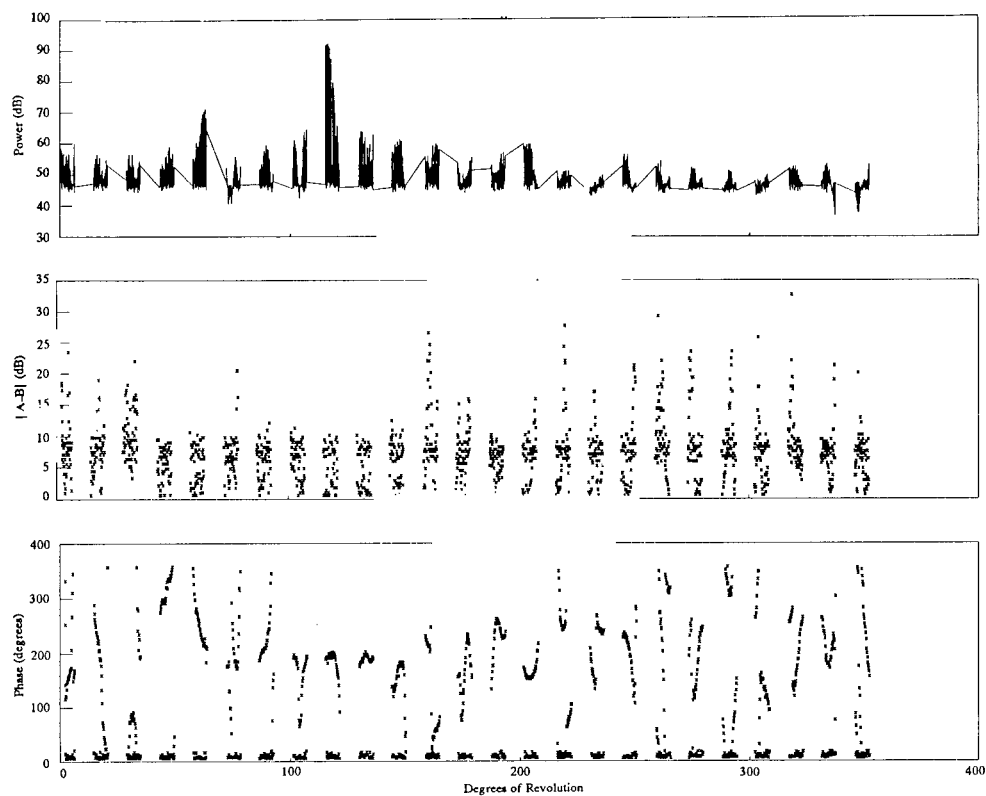Fig. 31—Example of data collected for the FR602D radar

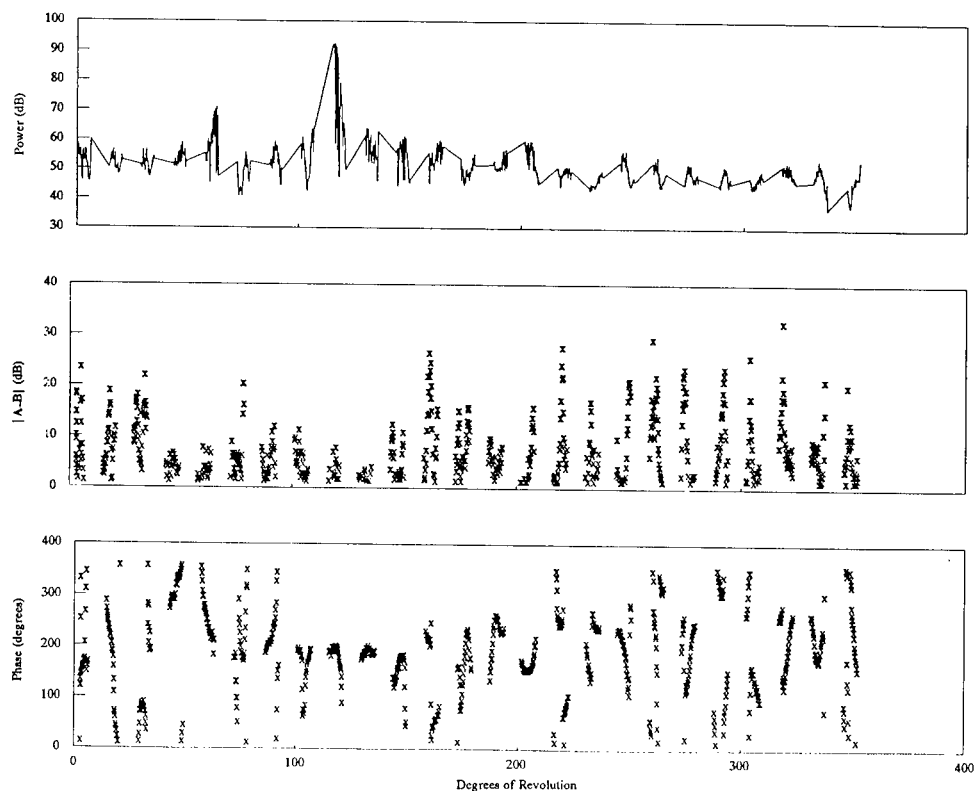Fig. 32 (a)—Sample of nonsorted data from the FR602D radar

Fig. 32 (b)—Sample of sorted data from the FR602D radar

and the other three sets of data collected 21 s of data, equivalent to about 8 revolutions of the radar

$$(24 \text{ rev}/1 \text{ min}) \times (1 \text{ min}/60 \text{ s}) \times 21 \text{ s} = 8.4 \text{ rev.}$$

These collection times were not chosen for any particular reason other than to collect enough scans for comparison. The radars were first measured from position 3, then from position 2, and finally from position 1. The vessels were pointing South while in all positions, although the exact angle heading was not measured. Therefore, the approximate angular separations between the pointing direction of the polarimeter antenna and the compass heading of the boat for the three positions are approximately 50° for position 3, 90° for position 2, and 130° for position 1. Figure 21 shows how these angles were approximated.

Test Results

Furuno FR8100 radar in position 3 - The first set of results presented from this phase of the test will compare two scans from a single radar while located in the same position. The antenna polarization characteristics of the first and second revolutions of the Furuno FR8100 radar in position 3 (data file 8260720.dat) are shown in Fig. 33. Recall from Section 4.7 and Fig. 20 that for a horizontally polarized antenna, the difference of the two components in amplitude is approximately 0 dB (because the two components are equal) and the time-phase difference between the two components is 180°.

Two observations are made from an initial look at the data in Fig. 33. First, the polarization characteristics are approximately the same for both revolutions, in that the difference-in-amplitude data at higher power levels are somewhere between 0 and 5 dB, and the time-phase measurements for these pulses are approximately 180°. These measurements indicate strong horizontally polarized pulses. The second observation is that the polarimeter is not measuring horizontal polarization for the pulses in the lower-powered sidelobes. This is evident from the fluctuation of the difference-in-magnitude data between 1 and 25 dB and the variation in the time-phase data between 0° and 360°. These characteristics agree with the theory on dipole polarization discussed earlier in this report in that the ratio of the copolarization component to the cross-polarization component of the electromagnetic wave transmitted from the dipole decreases as the power from the dipole decreases and, hence, the polarization changes.

In the second revolution of the radar, it is not evident where the mainbeam is located. This is caused by the 50 ms processing time of the polarimeter. The FR8100 radar, and all navigation radars measured during these tests, rotate at 24 rpm. At this rate of rotation, the radar has rotated 7.2° ((24 rev/1 min) × (360°/1 rev) × (1 min/60 s) × 50 × 10⁻³ s) during the 50 ms of polarimeter processing time. Recalling that this radar has a horizontal beamwidth of 1.23°, the polarimeter's processing time is enough to miss the mainbeam of the radar. However, one can tell where the mainbeam is by comparing the patterns of the antenna polarization characteristics of the two revolutions.

Furuno FR602D radar on Prince in position 2 - The second set of plots discussed in this section of the test show the similarities between two scans of the FR602D radar on the *Prince* in position 2 (Fig. 34). Part (a) of the figure is the first revolution of data file 8260919.dat and part (b) is the fifth, and last, revolution of the same data file.
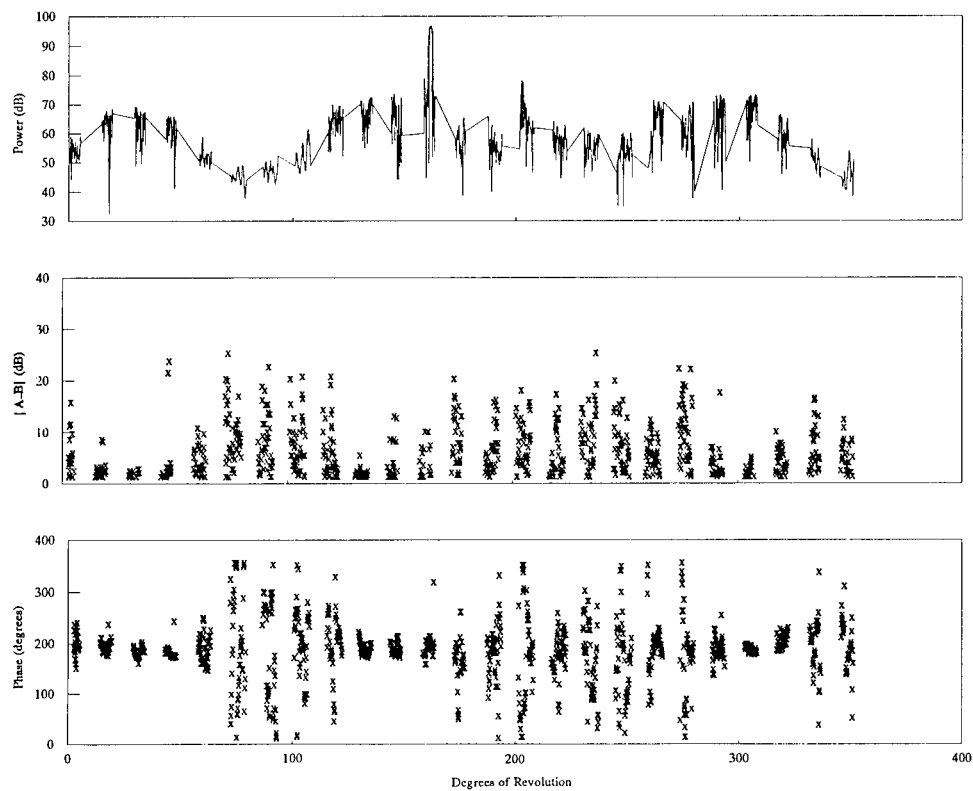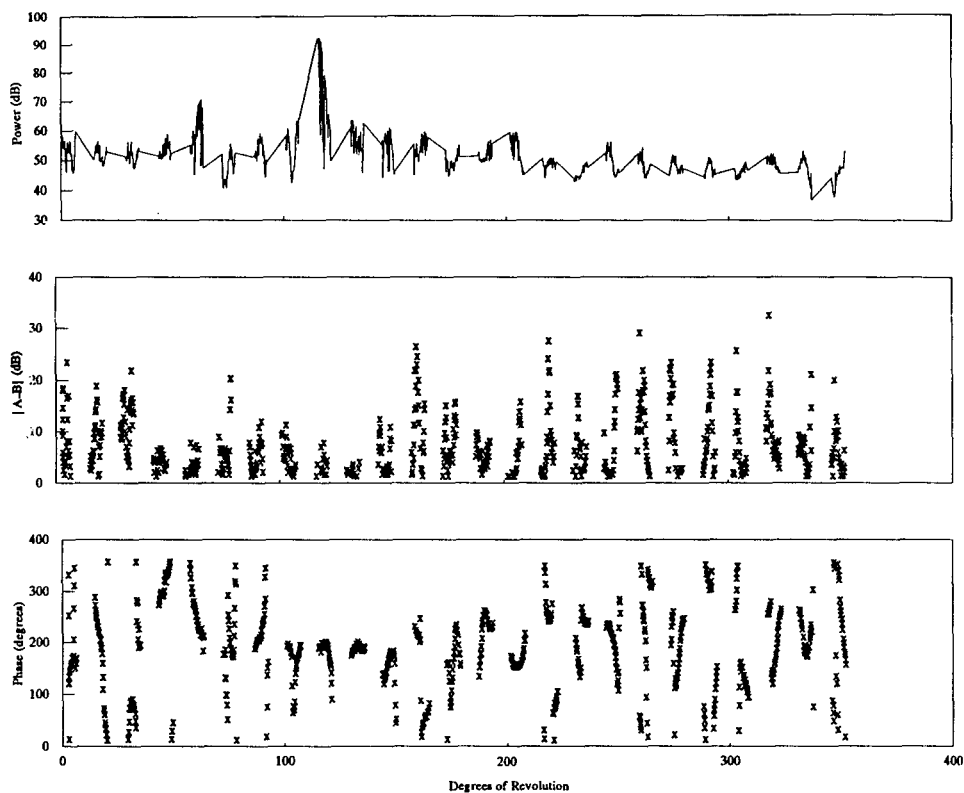
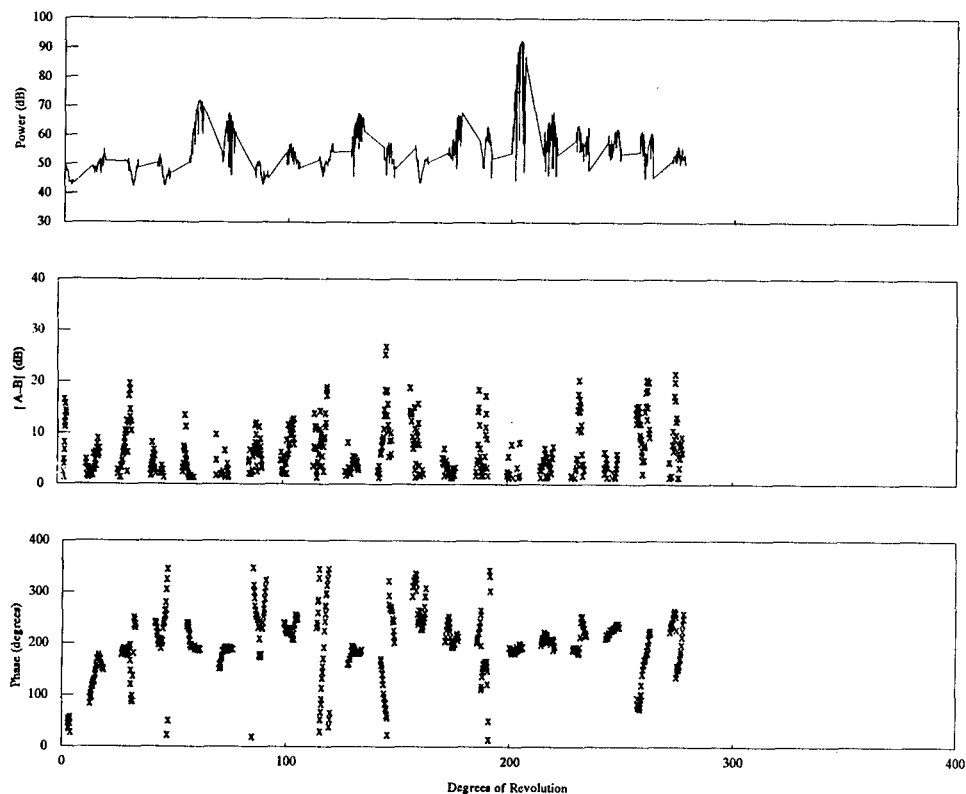(a) 1st revolution of data file 8260720.dat in position 3
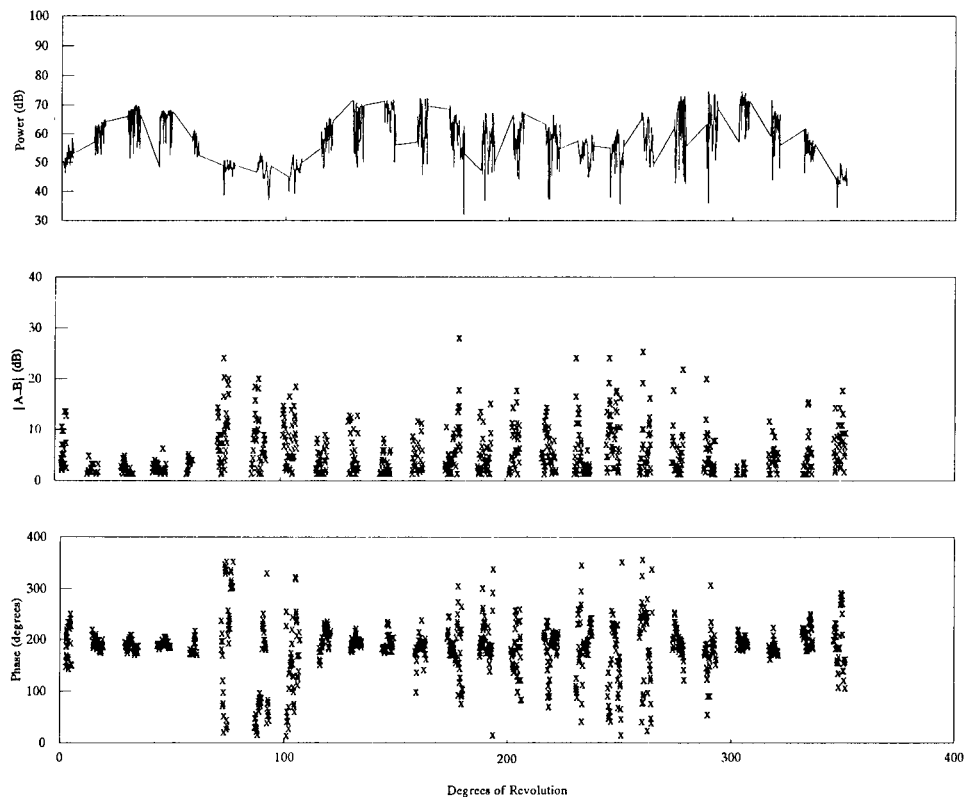
(b) 2nd revolution of data file 8260720.dat in position 3

Fig. 33—Scan-to-scan comparison of the FR8100 antenna sorted polarization data

(a) 1st revolution of data file 8260919.dat in position 2

(b) 5th revolution of data file 8260919.dat in position 2

Fig. 34—Scan-to-scan comparison of the FR602D sorted polarization data (*Prince*)

When comparing the two scans in Fig. 34, both the difference-in-magnitude data and the time-phase data have similar patterns. The difference-in-magnitude plot contains most datapoints between 0 and 10 dB. However, in some areas, primarily in the backlobes, the difference of the magnitude of the two components is larger by as much as 30 dB. This is a clear indication that some of the pulses in the backlobes are measured to be 45° or 135° slant polarizations.

A quick look at the time-phase measurements of this radar shows that they have a similar distribution. They appear to be highly concentrated around 180° in some areas of the revolution and random in other areas. A closer look at this parameter shows that the areas where the phase is close to 180° are where the high-powered pulses reside. In areas of the revolution where the power of the received signal is lower, the difference-in-magnitude and the time-phase data appear to be more random.

When comparing the data in Fig. 34 with the theory of copolarized and cross-polarized waves of edge-slotted waveguides, we see that the measured polarization characteristics of the FR602D radar agree with the theory. The electromagnetic field of the antenna at the mainbeam, where the power of the pulses is the highest, is highly copolarized (in this case horizontally). However, when the power of the signal drops, the polarization has a larger cross-polarized component and, hence, the polarization varies.

Furuno FR602D radar on Septar 06 in position 2 - Figure 35 shows two consecutive revolutions, the first and second, of the FR602D radar on the *Septar 06* in position 2. As in the FR602D radar on the *Prince*, the polarization characteristics vary in low-powered areas of the revolution and the signal is strongly horizontally polarized in higher-powered areas, such as in the mainbeam.

Conclusions

This scan-to-scan test demonstrated that, for the two measured radars, a radar can be identified from the polarization characteristics of a single scan of its antenna. A visual analysis of the data shows that the polarization characteristics for both radars follow a consistent pattern. The measured data verify the theoretical calculations for antenna polarization behavior in slotted waveguide antennas.

Phase II : Position-to-Position Antenna Characteristic Test

Procedures

The purpose of this phase of the test was to evaluate antenna polarization characteristics of the same radar antenna with the boat located in three different positions. The objective here was to see whether multipath affected the measured polarization. The antenna of the polarimeter was aimed at the vessel that carried the radar antenna being measured. The three locations of the vessel relative to the polarimeter antenna are discussed earlier in this report and are shown in Fig. 21. Six sets of data were collected, as in the previous phase: three sets of five antenna revolutions and three sets of eight antenna revolutions.
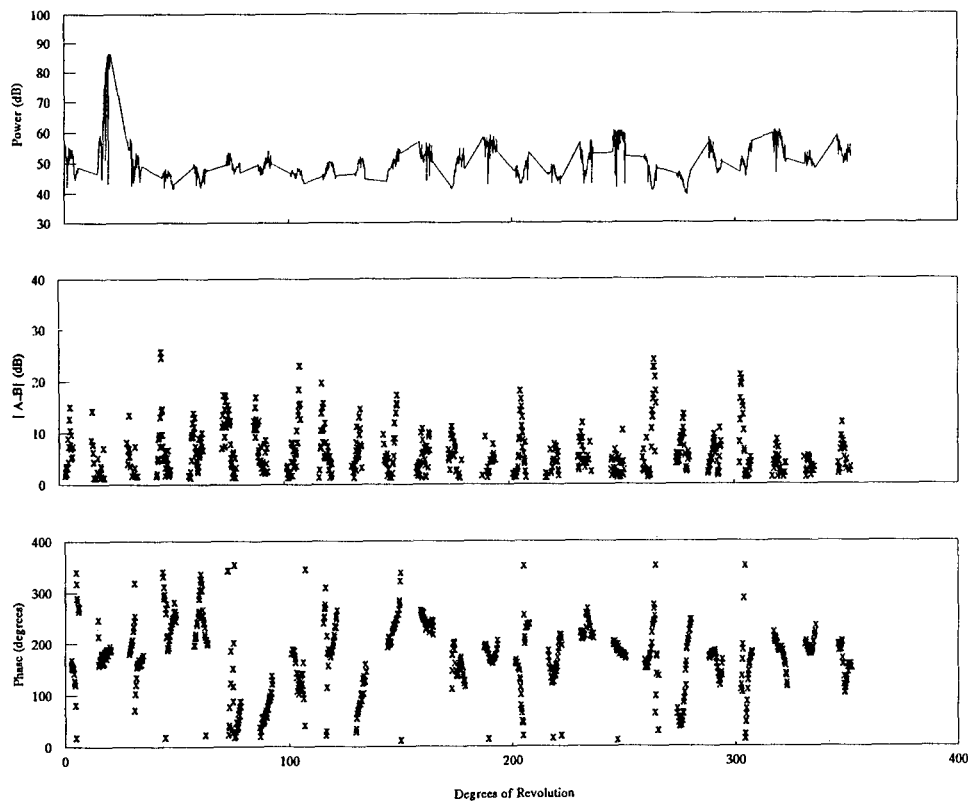
(a) 1st revolution of data file 8260822.dat in position 2
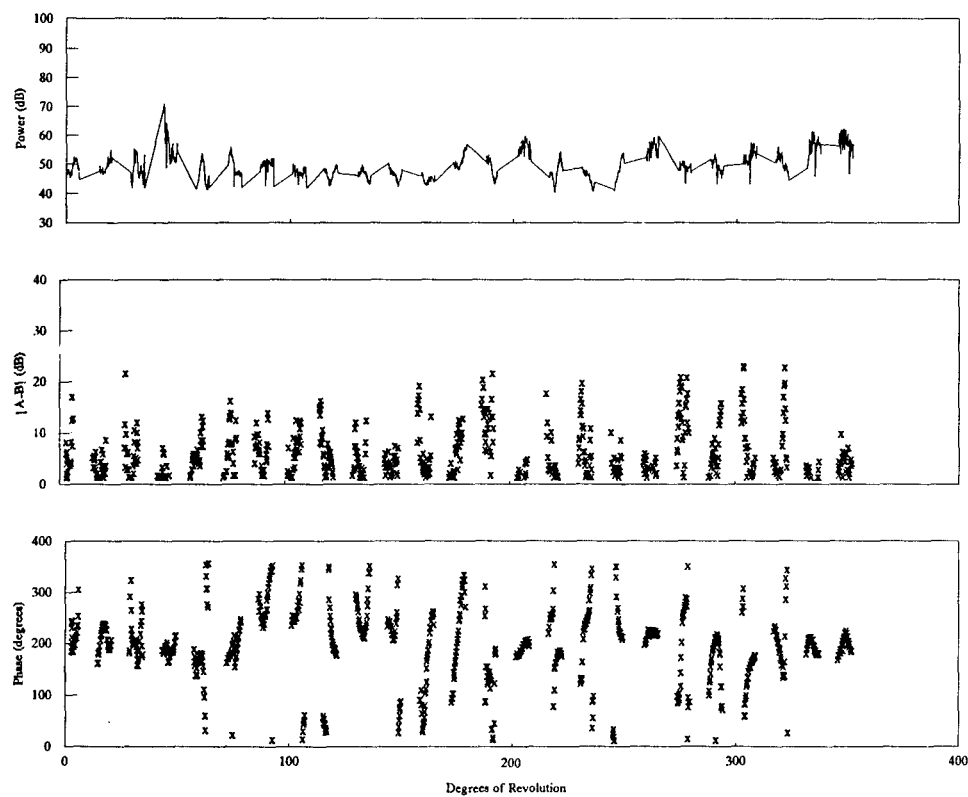
(b) 2nd revolution of data file 8260822.dat in position 2

Fig. 35—Scan-to-scan comparison of the FR602D sorted polarization data (*Septar 06*)

Test Results

Furuno FR8100 radar - Figure 36 shows the antenna polarization characteristics for the FR8100 navigation radar from the three different locations. Parts (a) through (c) of the figure shows the characteristics from positions 1 through 3, respectively. As can be seen in the plots, the polarization characteristics follow approximately the same pattern in all positions and, hence, the radar can be identified as potentially the same radar despite the location. The data indicate a strong horizontally polarized emitter in areas where the power from the emitter is highest. In areas of lower received power, the measurements show other polarizations where the cross-polarization component has become stronger. Environmental differences may account for the exceptions to this observation.

Furuno FR602D radar - A comparison of the FR602D radar antenna characteristics from the three positions was also made. Figure 37 illustrates revolutions of the FR602D antenna on the *Prince* from the three positions. Part (a) shows one of the third revolutions in position 1, part (b) shows one of the first revolutions in position 2, and part (c) shows one of the first revolutions in position 3. Figure 38 shows the antenna polarization characteristics of the FR602D radar on the *Septar 06* from the same three positions from which the data in Fig. 37 were collected.

Conclusions

Even though the basic pattern of the polarization characteristics is the same for each radar in the three positions, there are some slight variations throughout the revolutions. There are several possible explanations for these variations. One is that the orientation of the vessel relative to the polarimeter causes the field from the antenna to bounce off different objects on the vessel. The height of the antenna above sea level may also contribute to these differences. The FR8100 radar was higher than the FR602D radars and the boat that carried the FR8100 radar, the *Transporter*, is larger than the boats that carried the FR602D radars (i.e., the *Prince* and the *Septar 06*). The effects of these mounting variations need further consideration in the analysis of antenna polarization characteristics. A passing vessel may also cause a wake in the water's surface, which would change the multipath environment and affect the polarization of the electromagnetic wave. All of these uncertainties could be answered with further testing under stricter testing conditions.

Phase III : Radar-to-Radar Antenna Characteristic Test

Procedures

This phase of the test looked for differences in the polarization characteristics of different models of the same type of radar antenna. As discussed earlier, three navigation radars were measured: one Furuno FR8100 6.5-ft open-dome antenna (on the *Transporter*) and two Furuno FR602D closed-dome antennas (one on the *Septar 06* and the other on the *Prince*). All three antennas were measured in each location. The antennas were allowed to rotate continuously at a constant rate of 24 rpm and either five or eight revolutions of the antenna were collected per data file.
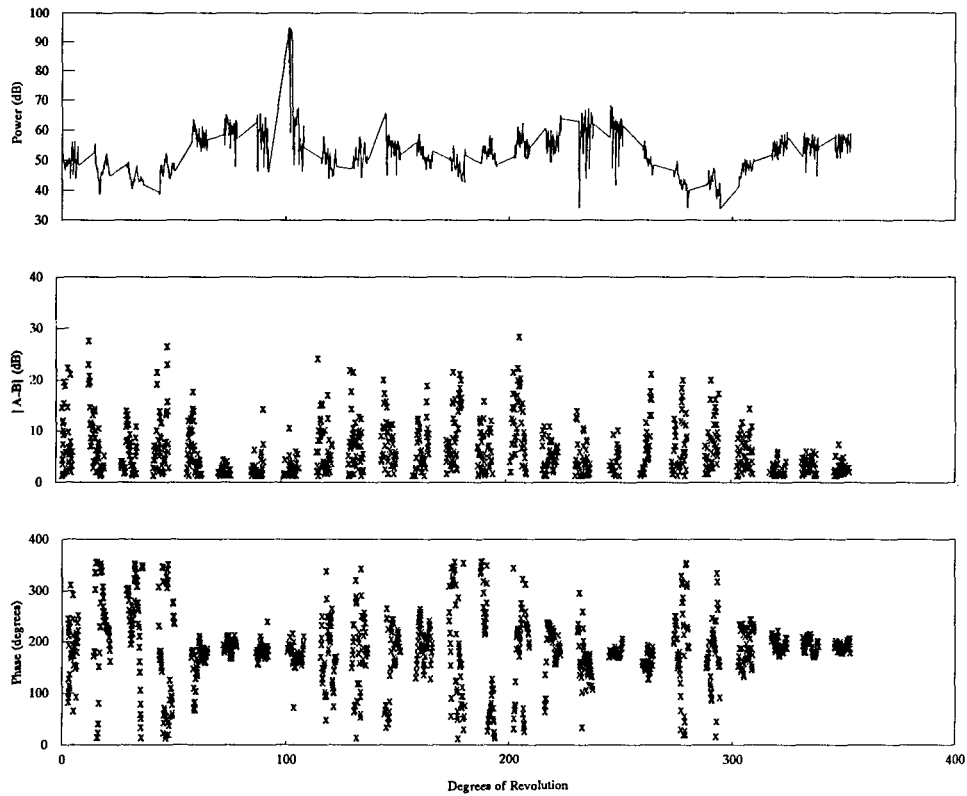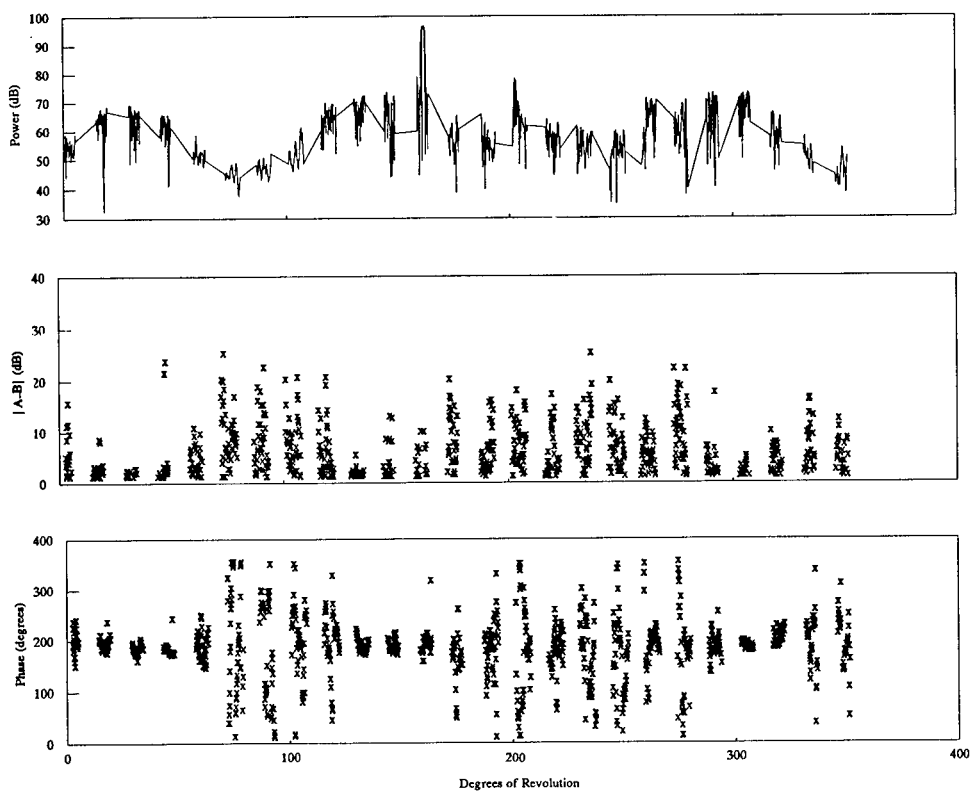
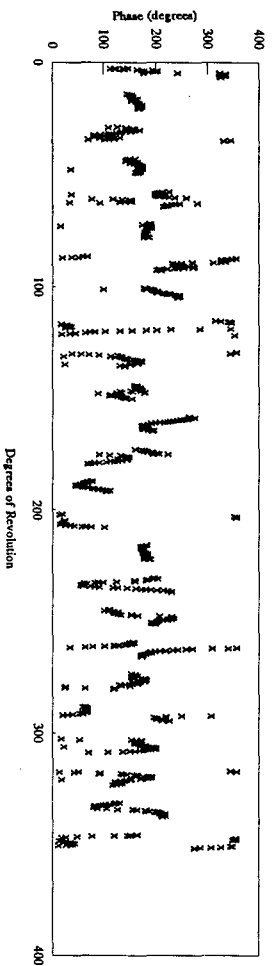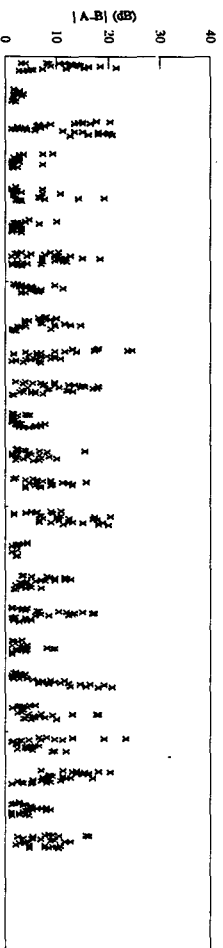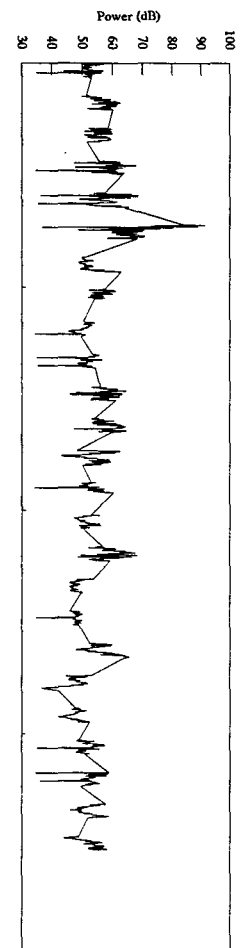(a) 1st revolution of data file 8260832.dat in position 1
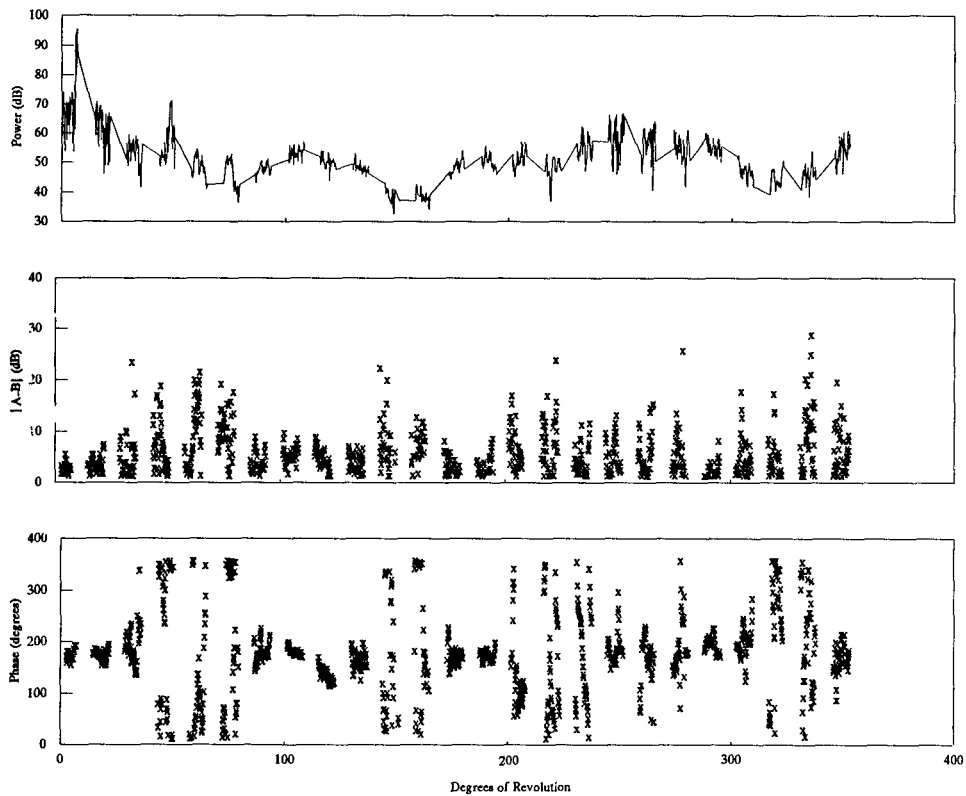
(b) 1st revolution of data file 8260804.dat in position 2

Fig. 36—Position-to-position comparison of the FR8100 sorted polarization data
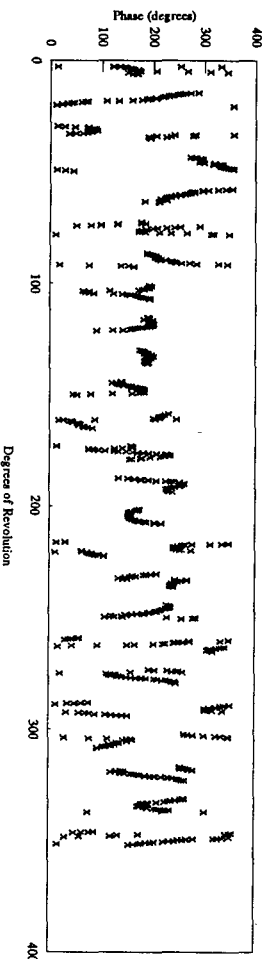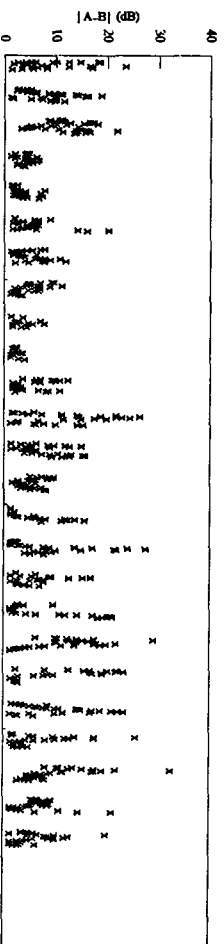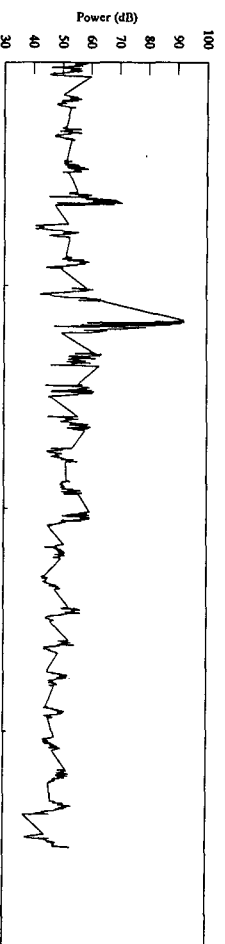
(c) 1st revolution of data file 8260720.dat in position 3

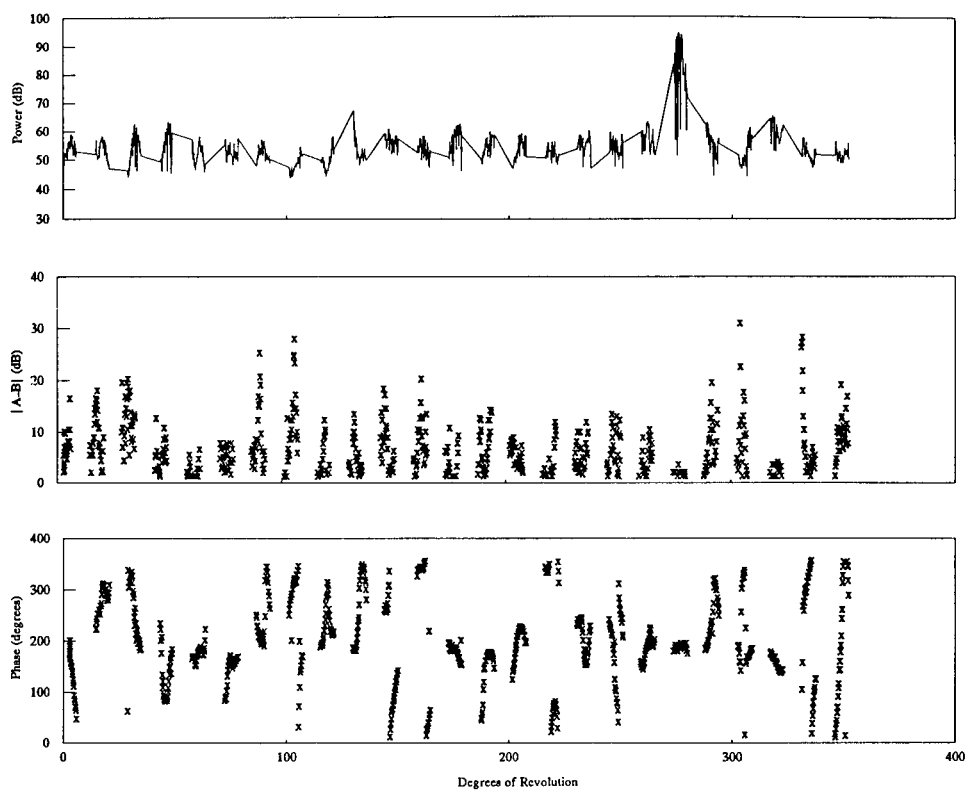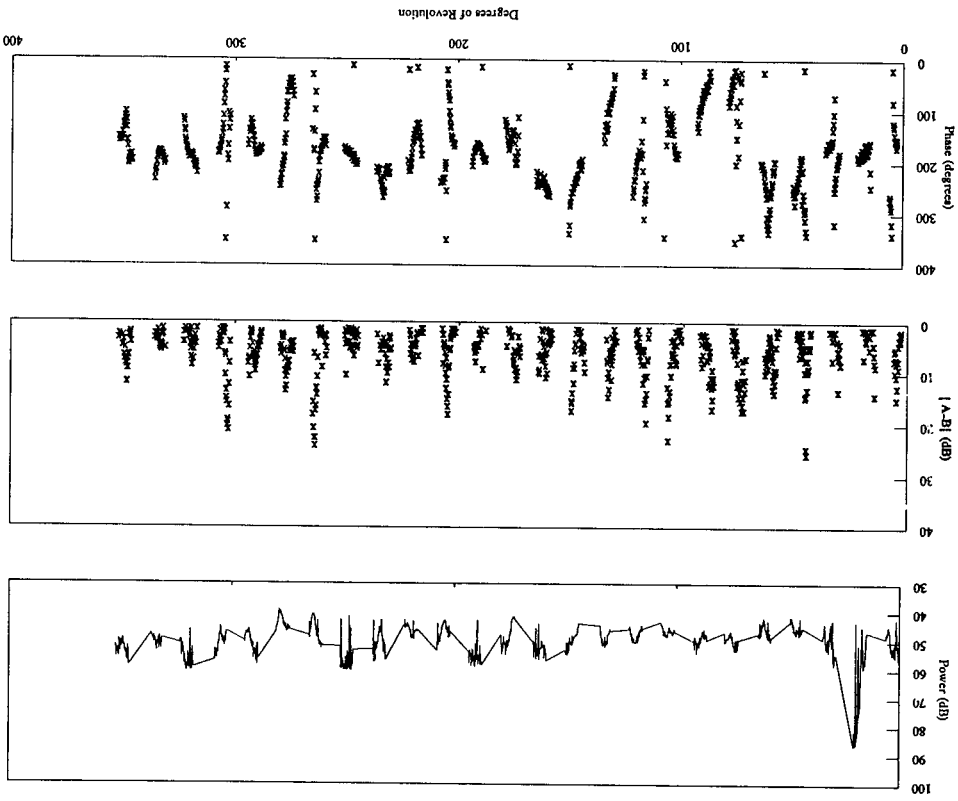Fig. 36 (cont.)—Position-to-position comparison of the FR8100 sorted polarization data

Power (dB)

| A-B| (dB)

Phase (degrees)

Degrees of Revolution

(a) 3rd revolution of data file 8260940.dat in position 1

Power (dB)

| A-B| (dB)

Phase (degrees)

Degrees of Revolution

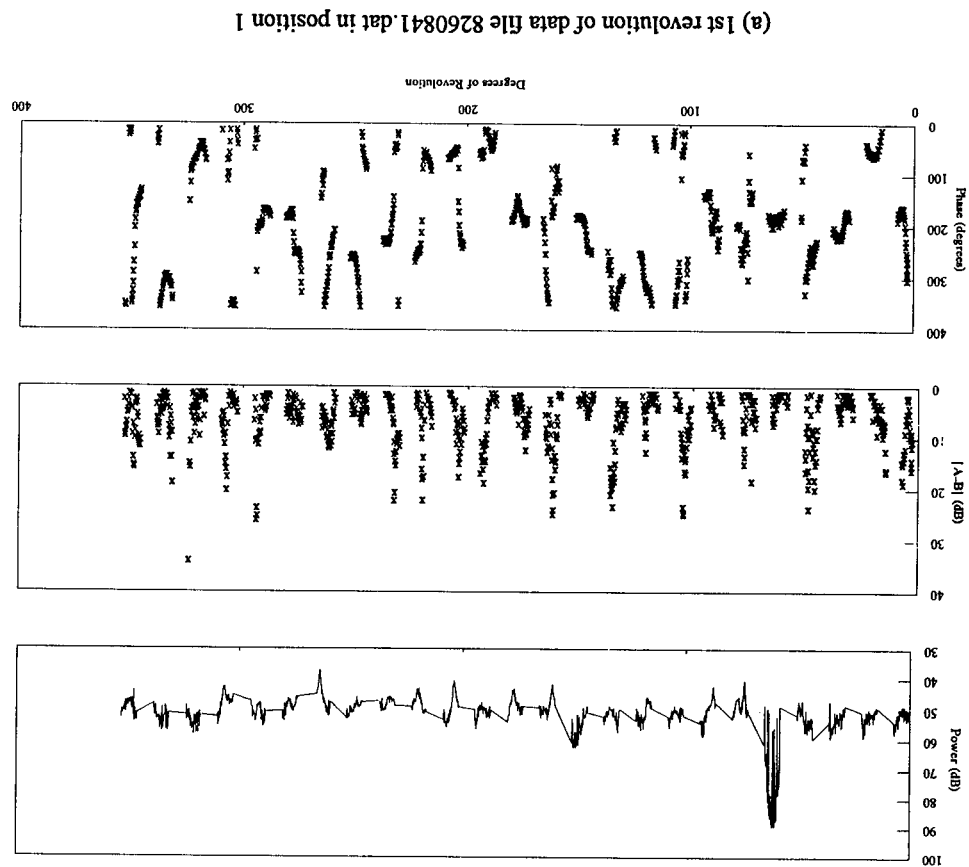(b) 1st revolution of data file 8260919.dat in position 2

Fig. 37—Position-to-position comparison of the FR602D sorted polarization data *(Prince)*

(c) 1st revolution of data file 8260901.dat in position 3

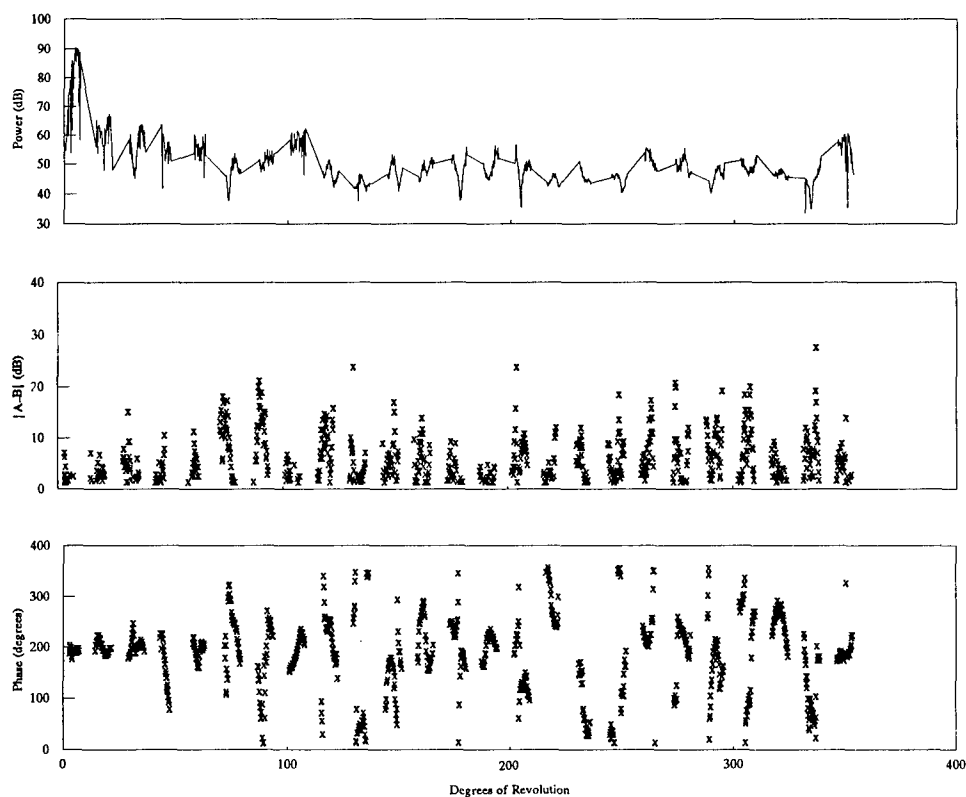Fig. 37 (cont.)—Position-to-position comparison of the FR602D sorted polarization data (*Prince*)

(c) 1st revolution of data file 8260758.dat in position 3

Fig. 38 (cont.)—Position-to-position comparison of the FR602D sorted polarization data (*Septar 06*)

Test Results

To demonstrate the results of this phase of the test, the polarization antenna characteristics of the first revolution of all three radars in position 2, shown in Fig. 39, were compared. Part (a) of the figure plots the polarimeter data of the FR602D radar on the *Septar 06*, part (b) shows the data of the FR602D radar on the *Prince*, and part (c) shows the data of the FR8100 radar on the *Transporter*.

As can be seen from Fig. 39, the antenna polarization characteristics of the FR602D radars are similar and those of the FR8100 radar are distinctly different from the FR602D. The best visual way to distinguish between the FR602D radar and the FR8100 radar is to look at the time-phase difference between the two polarization components.

Conclusions

A visual analysis of the antenna polarization characteristics of the two horizontally polarized navigation radars measured in this test concludes that they are different. The main factor contributing to these differences is the number of slots in the waveguide of the antenna. Theory says that the radiation from each slot in edge-slot waveguides has the same characteristics as dipoles [7]. As the number of dipoles and hence number of slots in the array increases, the ratio of copolarization to cross-polarization changes (the copolarization component decreases more rapidly with a larger number of elements). The slots in the Furuno radars are spaced approximately 2 cm apart. The elements in the 24 in.-diameter closed-dome radar occupy approximately 20 in. of the dome (approximately 25 slots) and the elements for the 6.5 ft open-array radar occupy almost the entire length of the array (approximately 100 slots).

Other differences in the design of the radars that may be contributing factors to the polarization characteristics of the antenna are

a) dome features (the FR8100 open-dome radar vs the closed-dome FR602D radar)
b) horizontal beamwidth (1.23° for the FR8100 radar and 2.5° for the FR602D radar)
c) location of the electronics for each radar; the electronics in the open array radars are contained in a metal case that shields the receiver from other RF sources.

The effects of these factors on polarization characteristics merit further investigation. The characteristics from these radars should be compared to those of other radars. By collecting more data from other radars under the same operational conditions, the conclusions made from this test can be validated.
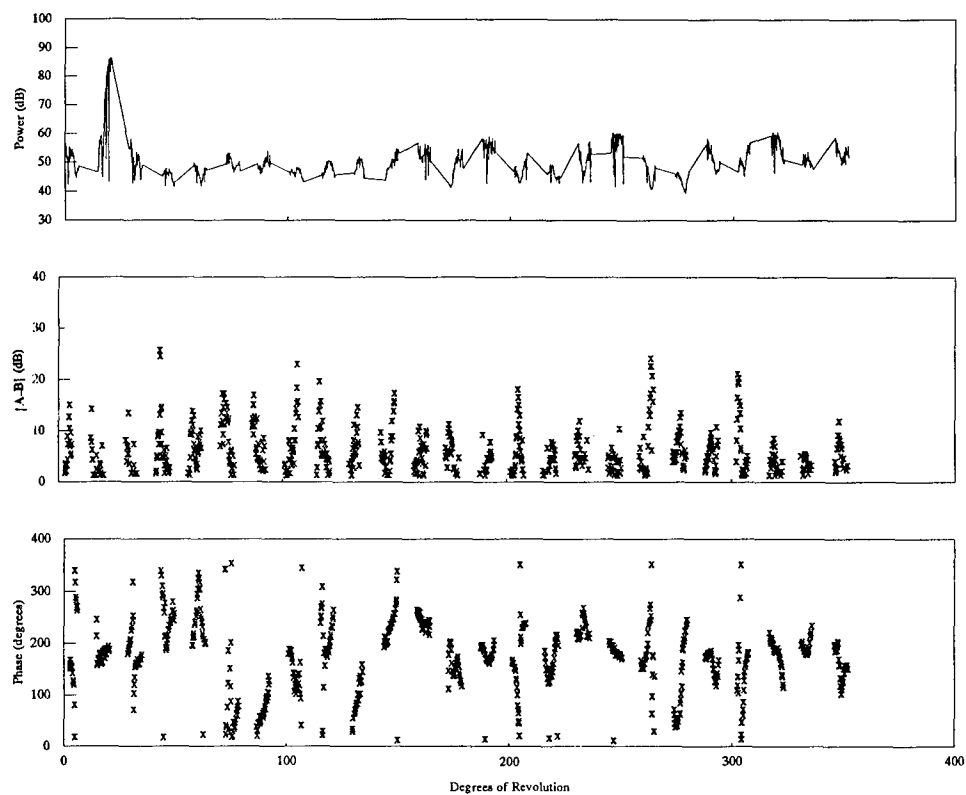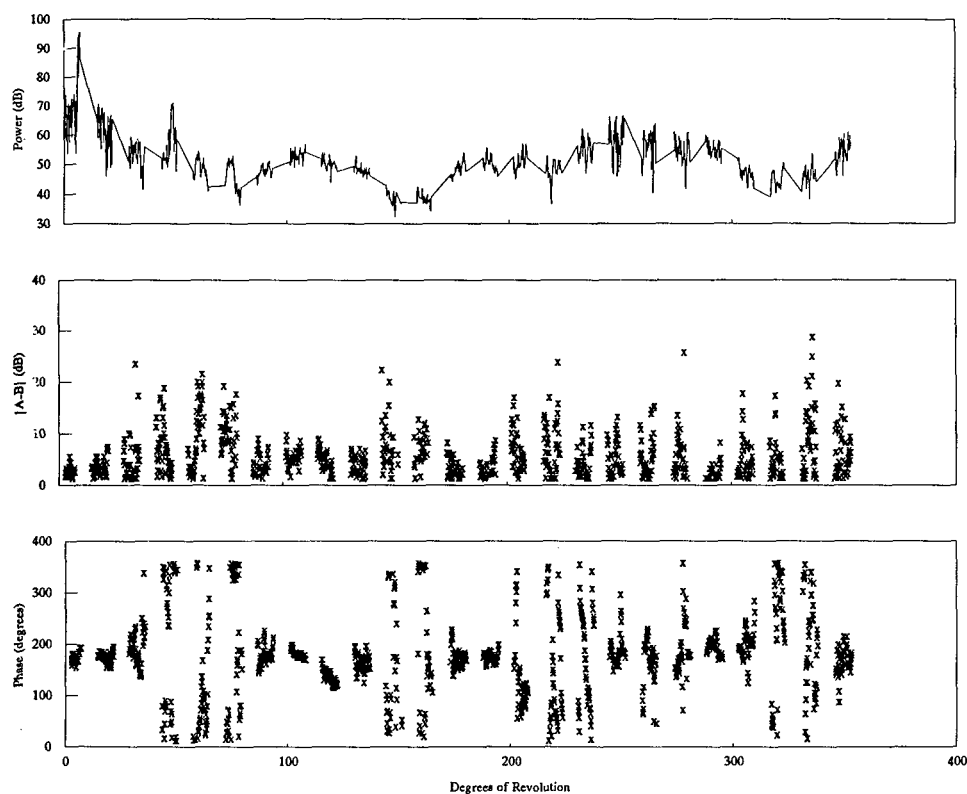
(a) FR602D radar on *Septar 06* - 1st revolution of data file 8260822.dat in position 2
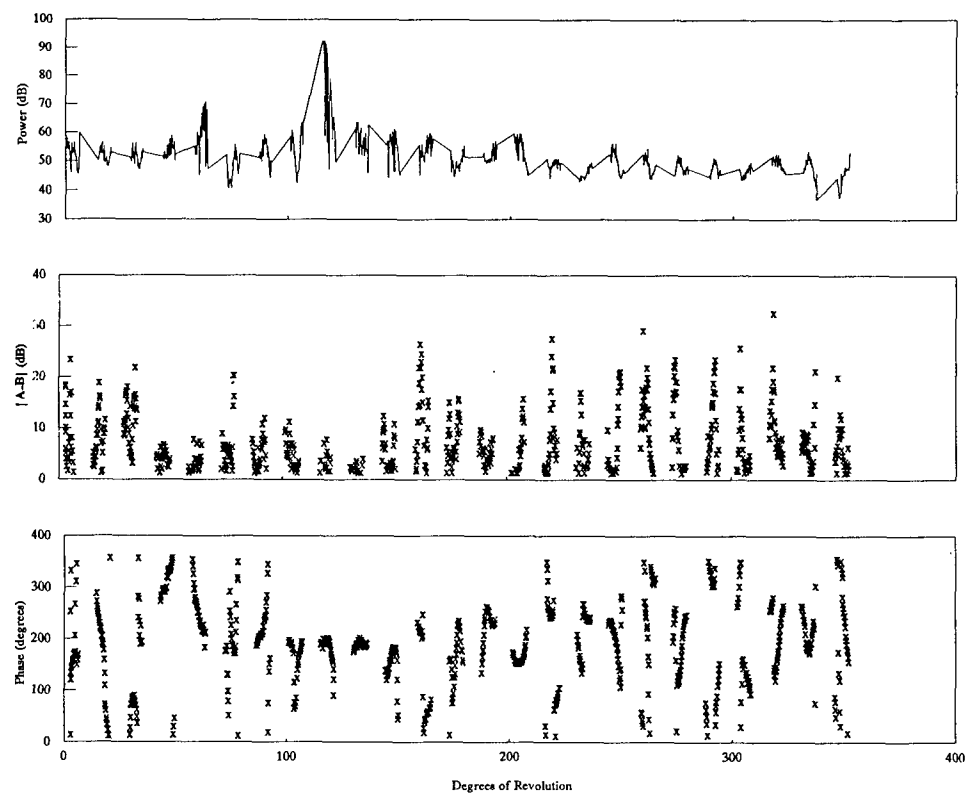
(b) FR602D radar on *Prince* - 1st revolution of data file 8260919.dat in position 2

Fig. 39—Radar-to-radar antenna polarization comparison (sorted data)

(c) FR8100 radar on _Transporter_ - 1st revolution of data file 8260804.dat in position 2

Fig. 39 (cont.)—Radar-to-radar antenna polarization comparison (sorted data)

6. CONCLUSIONS

The series of antenna characterization tests performed at the Naval Air Warfare Center - Aircraft Division (NAWC-AD) at Patuxent River, MD contributed significant insight into using antenna polarization as a means of radar recognition. The test approach was to evaluate radar characteristics from scan to scan, position to position, and between one another. Three navigation radars were measured, two of them of similar design but with different model numbers (Furuno FR602D 24-in. closed-dome radars) and the third one of different design (Furuno FR8100 6.5-ft open-dome radar).

The conclusions drawn from the data collected from the test documented in this report are based on a sorting routine developed to eliminate interfering signals and a visual analysis of the polarization characteristics as collected with the polarimeter.

The first phase of the test evaluated the consistency of the antenna polarization characteristics from a single radar. This was done by comparing multiple scans from the same unit. The results from the scan-to-scan test show that the scans from the same radar unit possess the same polarization characteristics with only slight variations in the sidelobes. This conclusion was based on a visual analysis of the results from the time-phase measurements (between orthogonal polarization components).

Two FR602D radars were measured in this test. From this test alone, it is not possible to discern from which of the two FR602D radars a signal originated. Better controlled tests may reveal differences in polarization characteristics between two units (i.e., different serial numbers) of the same radar model.

The next series of tests evaluated the similarities and/or differences in antenna polarization characteristics with the radars located at different positions relative to the polarimeter. The conclusion from this test is that the polarization characteristics look approximately the same for each radar in all positions. However, there are some slight variations throughout the revolutions. These variations may be caused by either the orientation of the boat relative to the polarimeter while in each position or the environment surrounding the radar in the different positions. Both of these features merit further investigation.

The most important comparison of characteristics made from this test was between same type but different model radars. A visual comparison of the antenna polarization characteristics of the FR8100 radar to those of either of the two FR602D radars reveals that the polarization characteristics are significantly different. The main reason for the differences is the number of slots in the waveguide of the antennas. The radiation from each slot behaves as a dipole. When dipoles are connected in series to form an array, the number of dipoles affects the copolarization-to-cross-polarization ratio. The more elements in the array, the more rapidly the copolarized component decreases with respect to angular distance from the mainbeam. Therefore, the polarization of the wave in the sidelobes changes continuously. The FR602D radar has approximately 25 slots in its waveguide, whereas the FR8100 radar has about 100 slots. This difference in radar design has an effect on the polarization characteristics.

Other differences in the design of the radars that may be contributing factors to the polarization characteristics of the antenna are

a) dome features (the 8100 open dome radar versus the closed dome FR602D radar)
b) horizontal beamwidth (1.23° for the 8100 radar and 2.5° for the FR602D radar)
c) location of the electronics for each radar; the electronics in the open array radars are contained in a metal case that shields the receiver from other RF sources.

The effects of these factors on polarization characteristics merit further investigation.

7. RECOMMENDATIONS

The following tests are recommended to be completed as a result of the test described in this report.

• The orientation of the boat on which a radar is being measured may affect the polarization of the electromagnetic wave transmitted from the radar. A series of tests should be conducted in which a boat is pointing at different angles relative to the polarimeter and a measurement of the radar is made while the boat is stationary in each orientation. These tests will help to determine how the reflections off different objects of the boat affect the polarization of the onboard radar antennas measured.

• It is known that radomes affect the polarization of fields passing through them. As a follow-up to the test discussed in this report, the polarization characteristics of the closed-dome antenna (FR602D) should be evaluated with and without the dome and the results compared. This test will determine just how much the dome affects the polarization of the transmitting field.

• Several tests can be conducted to evaluate the effects of multipath. One is to perform a chamber test and measure the same radars in a multipath-free environment. The second option is to do a follow-up test to measure the same radar at different heights above the water's surface.

• The radar antenna characteristics from the radars measured in this test should be compared to those of other radars to better evaluate the radar-to-radar characterization results. By collecting more data from other radars under the same operational conditions, the conclusions made from this test can be validated.

ACKNOWLEDGMENTS

REFERENCES

1. Synthetic Aperture Radar Technology and Application, Course 9223, University of Michigan, Ann Arbor, MI, Engineering Summer Conference Course, co-chairmen Dr. Adam Kozma and Dr. Robert A. Schuchman, July 1992.

2. M. Gherardelli, "Adaptive Polarisation Suppression of Intentional Radar Disturbance," *IEE Proc.*137 F(6), Dec. 1990.

3. E. Krogager, "Decomposition of the Sinclair Matrix into Fundamental Components with Application to High Resolution Radar Target Imaging," IEEE National Telesystems Conference 1991, Atlanta, GA.

4. M.I. Skolnik, *Introduction to Radar Systems* (McGraw Hill, New York, 1980) pp. 434-438.

5. Technology Service Corporation Training Course: "Modern Antenna," Naval Research Laboratory, 1993, Washington, D.C.

6. B.P.Lathi, "Analysis and Transmission of Signals," in *Modern Digital and Analog Communication Systems* (CBS Publishing, 1983), Chap. 2.

7. R. S. Elliott, "The Design of Waveguide-fed Slot Arrays," in *Antenna Handbook: Theory, Applications, and Design*, Y.T.Lo and S.W. Lee, eds. (Van Nostrand Reinhold Company, New York, 1988) Chap. 12, pp. 12-1 through 12-38.

8. "The Handbook of Antenna Design," Vol. 1, A. W. Rudge, K. Milne, A. D. Olver, and P. Knight, eds. (Peter Peregrinus Limited, U.K., 1982).

Appendix
DERIVATION OF FREQUENCY SPECTRUM REPRESENTATION

45° SLANT WAVE

For a 45° slant wave received on a dual-polarized antenna followed by a switch oscillating between the two orthogonal (in this case V and H) ports, the amplitude of the signal out of the sampler is constant and has a magnitude equal to 3 dB less than the power of the radar. The phase of the signal out of the sampler (i.e., the phase difference between either component and the incident wave) is 0° since the signals from the two ports are in-phase with one another and with the incident wave. Figure A1 shows the output from the sampler for a 45° slant polarized wave.
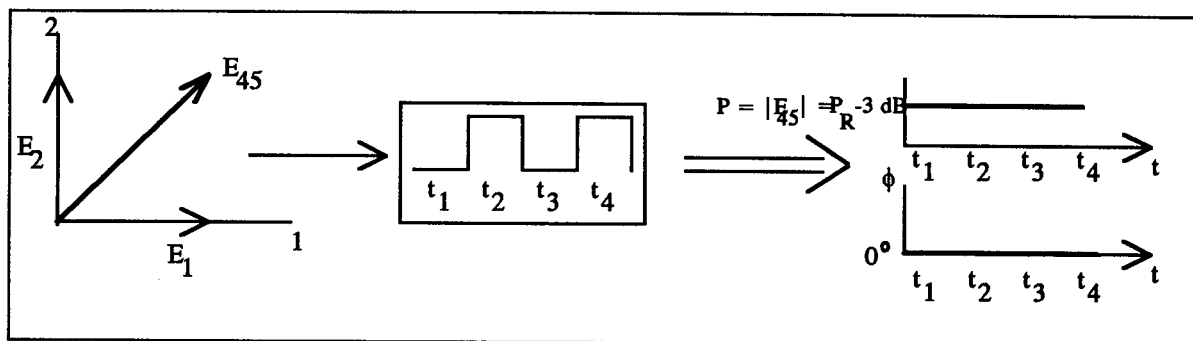

Fig. A1—Output from sampler for a 45° slant polarized wave

The real part of the signal out of the sampler is $P\cos\varphi = P\cos 0° = P$, and the imaginary portion is $P\sin\varphi = P\sin 0° = 0$, as shown in Fig. A2.
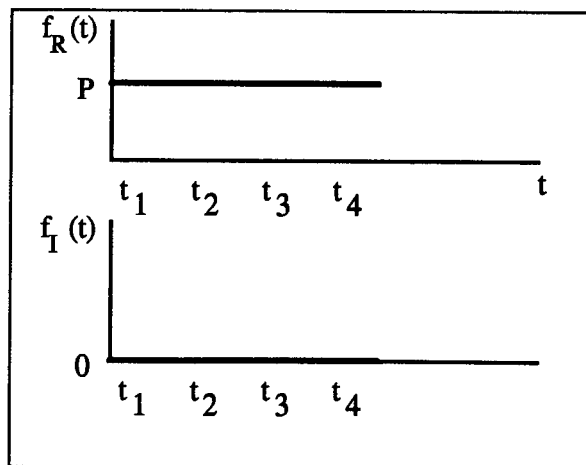

Fig. A2—Real and imaginary signals at sampler output for a 45° slant polarized wave

Any periodic signal can be expressed as a sum of sinusoids of frequencies 0, ω, 2ω,..... The periodic function can then be expressed as

$$g(t) = a_0 + \sum_{n=1}^{\infty} a_n \cos n\omega\, t + b_n \sin n\omega\, t \qquad (A1)$$

where the a's are the amplitudes of the cosine harmonics and the b's are the amplitudes of the sine harmonics. If the function is integrated over one period, the harmonics of the function can be found as follows:

$$a_0 = \frac{1}{T_0} \int_{t_0}^{t_0+T_0} f(t)dt \qquad (A2)$$

$$a_n = \frac{2}{T_0} \int_{t_0}^{t_0+T_0} f(t)\ \cos n\omega\, t dt \qquad (A3)$$

$$b_n = \frac{2}{T_0} \int_{t_0}^{t_0+T_0} f(t)\ \sin n\omega\, t dt, \qquad (A4)$$

where $\omega = 2\pi f = \dfrac{2\pi}{T_0}$.

For the real portion of the signal, $f(t) = P$. Substituting this in Eq. (A2) gives

$$a_0 = \frac{1}{T_0} \int_{t_0}^{t_0+T_0} P dt = \frac{P}{T_0}\left[(t_0 + T_0) - t_0\right] = P. \qquad (A5)$$

Substituting $f(t)$ into Eq. (A3) and using the sine identity, $\sin(A+B) = \sin A \cos B + \cos A \sin B$,

$$a_n = \frac{2}{T_0} \int_{t_0}^{t_0+T_0} P\cos\frac{2\pi n}{T_0} t dt$$

$$= \frac{P}{n\pi}\left[\sin\left(\frac{2\pi n}{T_0}(t_0 + T_0)\right) - \sin\frac{2\pi n}{T_0}t_0\right]$$

$$= \frac{P}{n\pi}\left[\sin\frac{2\pi n t_0}{T_0}\cos 2\pi n + \cos\frac{2\pi n t_0}{T_0}\sin 2\pi n - \sin\frac{2\pi n t_0}{T_0}\right]$$

$$= 0.$$

The coefficient $a_n = 0$ because $\cos 2\pi n = 1$ for all n, making the first term $\sin(2\pi n t_0/T_0)$, which cancels with the last term. The second term is zero because $\sin 2\pi n$ is always zero for all n.

Substituting $f(t)$ in Eq. (A4) and using the cosine identity, $\cos(A+B) = \cos A \cos B - \sin A \sin B$, results in

$$b_n = \frac{2}{T_0} \int_{t_0}^{t_0+T_0} P \sin \frac{2\pi n}{T_0} t \, dt$$

$$= -\frac{P}{n\pi} \left[\cos\left(\frac{2\pi n}{T_0}(t_0 + T_0) \right) - \cos \frac{2\pi n}{T_0} t_0 \right]$$

$$= -\frac{P}{n\pi} \left[\cos \frac{2\pi n t_0}{T_0} \cos 2\pi n + \sin \frac{2\pi n t_0}{T_0} \sin 2\pi n - \cos \frac{2\pi n t_0}{T_0} \right]$$

$$= 0.$$

This result ($b_n = 0$) is verified by the fact that for an even function (i.e., $f(x) = f(-x)$) all b_n coefficients vanish. The coefficients of the imaginary part of this signal do not exist because the imaginary portion is zero.

Replacing the values derived above into Eq. (A1) results in $g(t) = P$. This periodic function indicates that no harmonics are in this signal. This means that there is no amplitude modulation and, hence, no sidebands. Therefore, the spectral representation for a 45° slant wave is composed of only a_0, a single spectral line with a magnitude of P at a single frequency, as shown in Fig. A3. This spectral component contains all of the information about the 45° slant component of any wave received. The magnitude of this signal is one of the polarimeter's outputs and is designated as magnitude B.
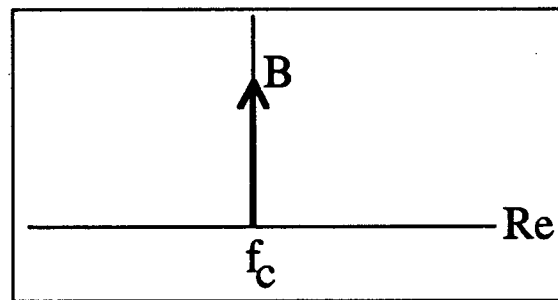

Fig. A3—Spectral component containing 45° slant information

The amplitude of the spectrum at a secondary frequency, if there were one, would be the magnitude of the second component. The third output of the polarimeter is the time phase difference between these two components. The time phase difference for a perfect 45° slant polarized wave is zero because both ports of the antenna are in phase with the 45° wave received. However, if this perfect wave is altered in polarization by multipath or other interferences, the time phase changes drastically because now there is a 135° slant component present that is 180° out of

phase. Therefore, the time phase difference of a 45° slant wave is undefined because it may vary depending on the amount of 135° slant component present.

135° SLANT WAVE

If a 135° slant wave is received on a VH dual-polarized antenna, as shown in Fig. A4, the vertical component of the wave is $+E_2$, and the horizontal component is $-E_1$, which, as referenced to antenna ports 1 and 2, is 180° out-of-phase with E_1. The phase of the signal out of the sampler is not constant, as shown in the figure. The amplitude of the signal from either port is the same and, therefore, in an ideal case, the amplitude of the signal out of the sampler is constant.
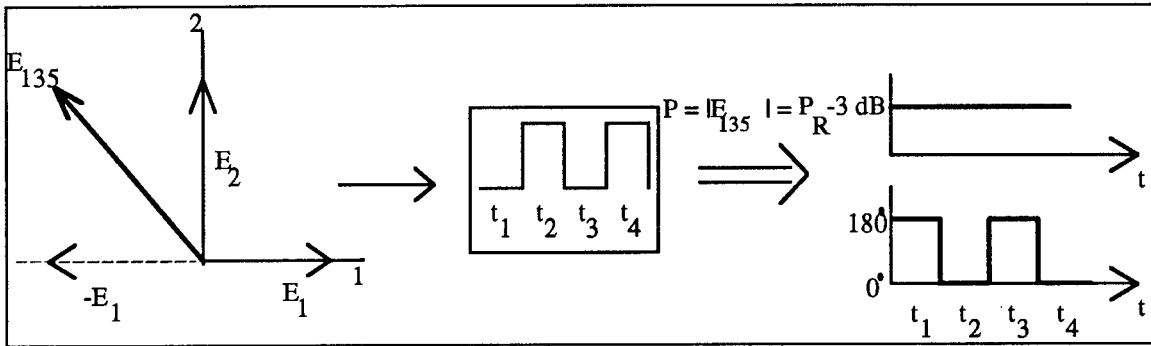

Fig. A4 —Output from sampler for a 135° slant-polarized wave

The real part of this sampled signal is

$$P \cos\varphi = P \cos 180° = -P \qquad \text{at } t = t_1, t_3, t_5, ...$$
$$P \cos\varphi = P \cos 0° \quad = P \qquad \text{at } t = t_2, t_4, t_6, ...$$

The imaginary portion is

$$P \sin\varphi = P \sin 180° = 0 \qquad \text{at } t = t_1, t_3, t_5, ...$$
$$P \sin\varphi = P \sin 0° = \ 0 \qquad \text{at } t = t_2, t_4, t_6, ...$$

The real and imaginary portions of the signal are illustrated in Fig. A5.
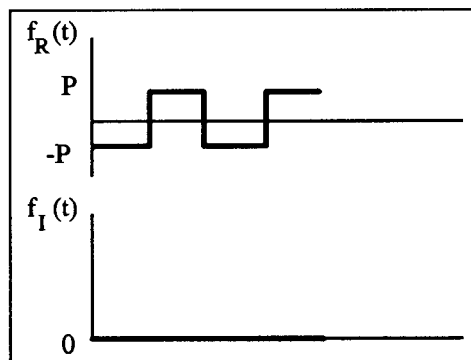

Fig. A5—Real and imaginary signals at sampler output for a 135° slant-polarized wave

Using the same equations as above, the a and b coefficients for the real part of the 135° slant polarized wave are

$$a_0 = \frac{1}{T_0}\left[\int_0^{\frac{1}{2}T_0} -P\,dt + \int_{\frac{1}{2}T_0}^{T_0} P\,dt\right]$$

$$= \frac{P}{T_0}\left[-\left(\frac{1}{2}T_0 - 0\right) + \left(T_0 - \frac{1}{2}T_0\right)\right] \tag{A8}$$

$$= 0,$$

and

$$a_n = \frac{2}{T_0}\left[\int_0^{\frac{1}{2}T_0} -P\cos\frac{2n\pi}{T_0}t\,dt + \int_{\frac{1}{2}T_0}^{T_0} P\cos\frac{2n\pi}{T_0}t\,dt\right]$$

$$= \frac{P}{n\pi}\left[-\left(\sin n\pi - 0\right) + \left(\sin 2n\pi - \sin n\pi\right)\right] \tag{A9}$$

$$= 0,$$

which satisfies the condition that for an odd function, such as $f_R(t)$ (i.e., $f(x) = -f(-x)$), all a_n coefficients vanish, and

$$b_n = \frac{2}{T_0}\left[\int_0^{\frac{1}{2}T_0} -P\sin\frac{2n\pi}{T_0}t\,dt + \int_{\frac{1}{2}T_0}^{T_0} P\,dt\right]$$

$$= \frac{P}{n\pi}\left[\left(\cos n\pi - \cos 0\right) - \left(\cos 2n\pi - \cos n\pi\right)\right] \tag{A10}$$

$$= \frac{P}{n\pi}\left[2\cos n\pi - 1 - \cos 2n\pi\right].$$

If n is an odd number,

$$b_n = \frac{P}{n\pi}\left[-2 - 1 - 1\right] = \frac{-4P}{n\pi},$$

and if *n* is an even number,

$$b_n = \frac{A}{n\pi}[2-1-1] = 0.$$

Since the imaginary portion of this signal is zero, no coefficients exist in the imaginary plane; all of the harmonics exist in the real plane. Replacing these values into Eq. (A1) gives the following periodic function for the 135° slant wave:
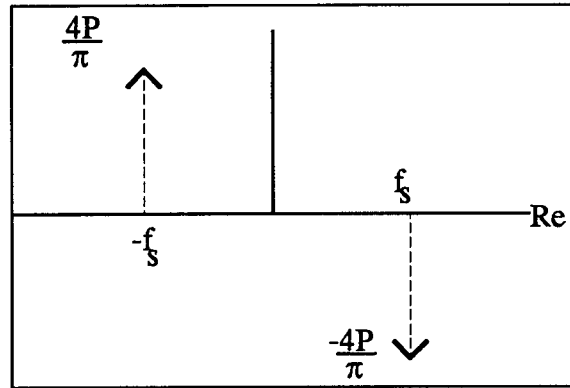
$$g(t) = \sum_{n=odd} \frac{-4P}{n\pi}\sin(n\omega t).$$

Fig. A6—Spectral components containing 135° slant information

This periodic function indicates that there is no signal at the primary frequency ($a_0 = 0$) and the only components are sine harmonics (indicated by the dotted lines Fig. A6) at odd frequencies. The magnitude of the harmonics at the negative frequencies are positive because $\sin(-\omega\,t) = -\sin(\omega\,t)$. These harmonics are demonstrated in Fig. A6.

VERTICAL WAVE

By following the same procedures as above, similar frequency domain representations of the polarimeter output can be derived for the other major polarizations (vertical, horizontal, right-hand circular, and left-hand circular). For vertical polarization, $a_0 = P/2$, $a_n = 0$, and $b_n = -2P/n\pi$ for odd harmonics and $b_n = 0$ for even harmonics in the real plane. There are no coefficients in the imaginary plane. The periodic function for vertical polarization is

$$g(t) = \frac{P}{2} - \sum_{n=odd} \frac{2P}{n\pi}\sin(n\omega\,t)$$

and the spectrum is illustrated in Fig. A7.

HORIZONTAL WAVE

For horizontal polarization, $a_0 = P/2$, $a_n = 0$, and $b_n = 2P/n\pi$ for odd harmonics and $b_n = 0$ for even harmonics in the real plane. There are no coefficients in the imaginary plane. The periodic function for horizontal polarization is

$$g(t) = \frac{P}{2} + \sum_{n=odd} \frac{2P}{n\pi} \sin(n\omega t)$$

and the spectrum is illustrated in Fig. A8.

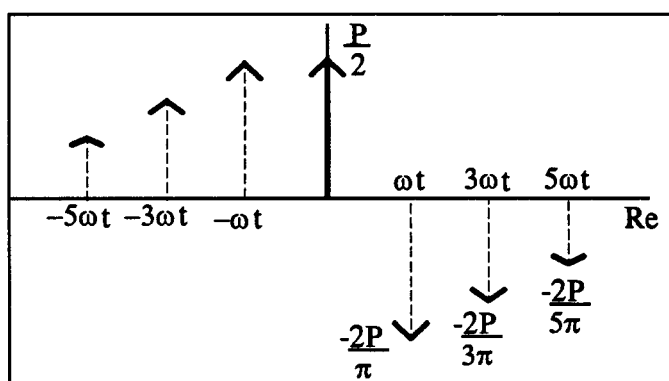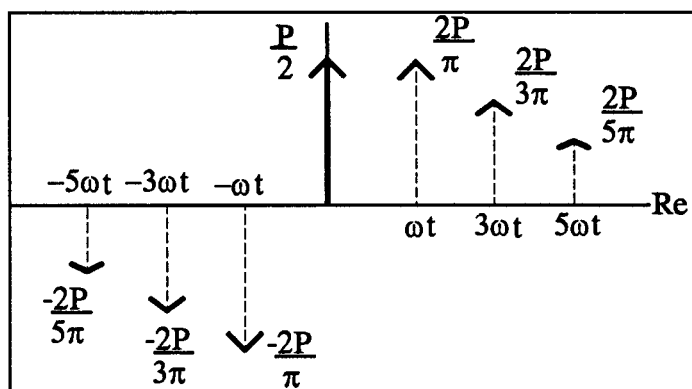Fig. A7—Spectrum for a vertical polarized wave

Fig. A8—Spectrum for a horizontal polarized wave

RIGHT-HAND CIRCULAR WAVE

For right-hand circular polarization, $a_0 = P/2$, $a_n = 0$, and $b_n = 2P/n\pi$ for odd harmonics and $b_n = 0$ for even harmonics in the real plane. In the imaginary plane, the coefficients are

$a_0 = P/2$, $a_n = 0$, and $b_n = 2P/n\pi$ for odd harmonics and $b_n = 0$ for even harmonics. Therefore, the periodic function for right-hand circular polarization in the real plane is

$$g(t) = \frac{P}{2} + \sum_{n=odd} \frac{2P}{n\pi} \sin(n\omega t)$$

and the function in the imaginary plane is

$$g(t) = \frac{P}{2} - \sum_{n=odd} \frac{2P}{n\pi} \sin(n\omega t).$$

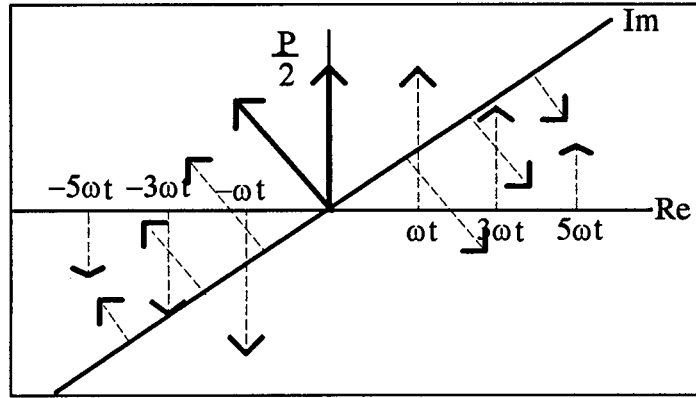The spectrum for right-hand circular polarization is illustrated in Fig. A9.

Fig. A9—Spectrum for a right-hand circular polarization

LEFT-HAND CIRCULAR WAVE

For left-hand circular polarization, $a_0 = P/2$, $a_n = 0$ and $b_n = 2P/n\pi$ for odd harmonics and $b_n = 0$ for even harmonics in the real plane. In the imaginary plane, the coefficients are $a_0 = -P/2$, $a_n = 0$, and $b_n = 2P/n\pi$ for odd harmonics and $b_n = 0$ for even harmonics. The periodic function for right-hand circular polarization in the real plane is

$$g(t) = \frac{P}{2} + \sum_{n=odd} \frac{2P}{n\pi} \sin(n\omega t)$$

and the function in the imaginary plane is

$$g(t) = -\frac{P}{2} + \sum_{n=odd} \frac{2P}{n\pi} \sin(n\omega t).$$

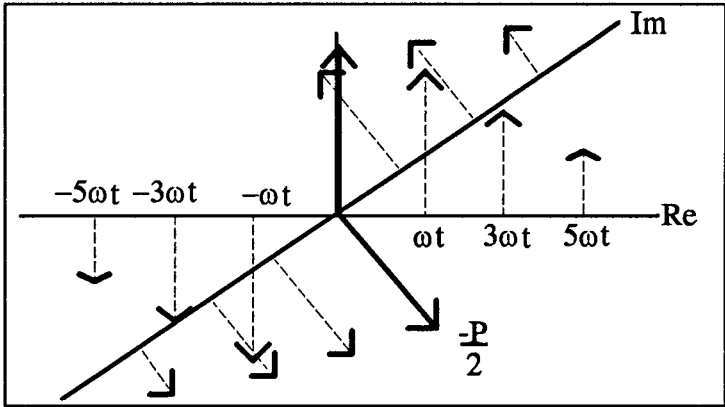The spectrum for left-hand circular polarization is shown in Fig. A10.

Fig. A10—Spectrum for left-hand circular polarization